

Statistical Benchmarking of Optimization Methods for Variational Quantum Eigensolver under Quantum Noise

Silvie Illésová*

*IT4Innovations National Supercomputing Center,
VSB - Technical University of Ostrava, 708 00 Ostrava, Czech Republic and
Gran Sasso Science Institute, L'Aquila, Italy*

Tomáš Bezděk

*Department of Mathematics, TUM School of Computation,
Information and Technology, Technical University of Munich,
Boltzmannstraße 3, D-85748, Garching b. München, Germany*

Vojtěch Novák

*Department of Computer Science, Faculty of Electrical Engineering and Computer Science,
VSB-Technical University of Ostrava, Ostrava, Czech Republic
IT4Innovations National Supercomputing Center,
VSB - Technical University of Ostrava, 708 00 Ostrava, Czech Republic and
Department of Informatics and Statistics, Marine Research Institute, Klaipeda University, Lithuania*

Bruno Senjean

*Institute Charles Gerhardt Montpellier, Université Montpellier,
CNRS, ENSCM, Route de Mende, 1919, Montpellier, France*

Martin Beseda

*Dipartimento di Ingegneria e Scienze dell'Informazione e Matematica,
Università dell'Aquila, Via Vetoio, I-67010 Coppito, L'Aquila, Italy and*

(Dated: March 23, 2026)

This work investigates the performance of numerical optimization algorithms applied to the State-Averaged Orbital-Optimized Variational Quantum Eigensolver for the H_2 molecule under various quantum noise conditions. The goal is to assess the stability, accuracy, and computational efficiency of commonly used gradient-based, gradient-free, and global optimization strategies within the Noisy Intermediate-Scale Quantum regime. We systematically compare six representative optimizers, BFGS, SLSQP, Nelder–Mead, Powell, COBYLA, and iSOMA, under ideal, stochastic, and decoherence noise models, including phase damping, depolarizing, and thermal relaxation channels. Each optimizer was tested over multiple noise intensities and measurement settings to characterize convergence behavior and sensitivity to noise-induced landscape distortions. The results show that BFGS consistently achieves the most accurate energies with minimal evaluations, maintaining robustness even under moderate decoherence. COBYLA performs well for low-cost approximations, while SLSQP exhibits instability in noisy regimes. Global approaches such as iSOMA show potential but are computationally expensive. These findings provide practical guidance for selecting suitable optimizers in variational quantum simulations, highlighting the importance of noise-aware optimization strategies for reliable and efficient quantum chemistry computations on current hardware.

INTRODUCTION

Quantum computing is rapidly advancing as a promising computational paradigm for tackling problems that remain practically infeasible for classical computers due to *quantum advantage* [1–3]. Its well-known potential applications span quantum chemistry [4–9], physics [10–14], material design [15–20], software engineering [21–26], benchmarking [27–33], finance [34–39], and machine learning [40–47]. Among the available approaches, Variational Quantum Algorithms (VQAs) are particularly at-

tractive for the current Noisy Intermediate-Scale Quantum (NISQ) era, as they combine quantum state measurements with classical optimization, thus aiming for possible speedup, while leaving most computations to the classical infrastructure, avoiding decoherence.

A flagship example of VQAs is the Variational Quantum Eigensolver (VQE) [48, 49], designed to compute ground-state energies of physical systems. Recent extensions, such as the State-Averaged Orbital Optimized Variational Quantum Eigensolver (SA-OO-VQE) [50–52], broaden this scope to include excited states. This makes SA-OO-VQE a quantum equivalent of the classical MCSCF method [53], offering a systematic path toward excited-state calculations on quantum hardware.

As a starting point, we restrict our present study to

* silvie.illesova@seznam.cz

the dihydrogen molecule H_2 , the simplest nontrivial electronic system. Although elementary, H_2 provides an ideal benchmark for algorithm testing or basic numerical analysis due to its simple electronic structure, modest resource requirements, and relevance as the minimal model for chemical bonding. In subsequent work, the methodology developed here will be extended to more complex and chemically relevant molecules.

As the critical aspect of VQAs is their reliance on classical numerical optimization [54, 55], the efficiency and reliability of these algorithms ultimately hinge on the optimizer’s ability to navigate a high-dimensional, noisy cost function landscape [56–58]. This landscape is shaped by both the chosen ansatz and unavoidable imperfections such as sampling noise and different types of decoherence [59, 60]. Understanding how different optimization strategies behave in such environments is therefore essential for the practical implementation of not only VQAs, but also all algorithms on NISQ computers.

In this manuscript, we present a systematic numerical study of several optimization methods applied to SA-OO-VQE for H_2 , spanning gradient-based, gradient-free, and global strategies, directly continuing our previous works, focused both on SA-OO-VQE [50, 52] and the Variational Hamiltonian Ansatz approaches[6]. By analyzing the optimizers’ behavior under idealized conditions and various noise models, we identify their strengths, limitations, and also the specific effects of different types of noise. Eventually, we provide practical, general guidance for selecting optimizers in NISQ era quantum simulations based on extensive statistical tests of our results, so they also lay the groundwork for scaling to larger molecular systems in the following work.

The researched H_2 geometry, SA-OO-VQE method, the adopted optimization approaches, and the selected quantum estimators emulating different types of noise are described in Section I. It is followed by Section II, which contains all the numerical results comparing the efficiency of optimizers with respect to several different types of quantum noise and the subsequent statistical tests. Section III describes the software implementation and provides details and the link to the replication package. Finally, Section IV contains the conclusions, providing general advice for the numerical optimization in the environments with quantum noise, based on statistically significant results.

I. METHODOLOGY

This section presents the computational setup and methodological framework used in this study. The SA-OO-VQE formulation, the tested optimization algorithms, and the noise and estimator configurations used to assess their performance are described here.

A. SA-OO-VQE

In this work, we study the convergence of a VQE towards the ground- and first-excited-state energies of the H_2 molecule with an internuclear distance of 0.74279 Å, which directly corresponds to the bond length in the equilibrium geometry. The electronic structure was treated within the Complete Active Space (CAS) approximation using $CAS(n_{elec}, n_{orb}) = CAS(2, 2)$ and the correlation-consistent polarized valence double- ζ (cc-pVDZ) basis set. As a standard VQE relies on the Rayleigh–Ritz variational principle for the ground state only, we consider its extension to excited states based on the generalized variational principle for an ensemble of states, so-called the Theophilou–Gross–Oliveira–Kohn variational principle [61, 62], thus leading to the state-average orbital-optimized VQE (SA-OO-VQE) [7, 50–52, 63, 64] which is the quantum analog of the state-average multi-configurational self-consistent field (SA-MCSCF) on classical computers [65]. Within SA-OO-VQE, the cost function reads as follows,

$$E^{SA-OO-VQE} = \min_{\kappa, \theta} \left\{ \langle \Psi_A(\theta) | \hat{H}(\kappa) | \Psi_A(\theta) \rangle + \langle \Psi_B(\theta) | \hat{H}(\kappa) | \Psi_B(\theta) \rangle \right\} \quad (1)$$

$$\geq \langle \Psi_0 | \hat{H}(\kappa^*) | \Psi_0 \rangle + \langle \Psi_1 | \hat{H}(\kappa^*) | \Psi_1 \rangle,$$

where κ^* and θ^* denote the minimizing sets of parameters, and

$$|\Psi_A(\theta)\rangle = \hat{U}(\theta)|\Phi_A\rangle \text{ and } |\Psi_B(\theta)\rangle = \hat{U}(\theta)|\Phi_B\rangle \quad (2)$$

are prepared on the quantum computer using the circuit-parametrized ansatz $\hat{U}(\theta)$ (being the generalized unitary coupled-cluster ansatz with single and double excitations [66] and in our case consisting of 3 trainable parameters) applied on a set of two orthonormal initial states $|\Phi_A\rangle$ and $|\Phi_B\rangle$ (with $\langle \Phi_A | \Phi_B \rangle = 0$). In this work, the Hartree–Fock state and the first-excited singlet configuration state function were used for $|\Phi_A\rangle$ and $|\Phi_B\rangle$, respectively. The orbital dependence of the Hamiltonian in the active space approximation is represented by the parameters κ , and its derivation is well detailed in Ref. [50]. According to Eq. (2) and the variational principle [61, 62], the SA-OO-VQE energy is lower-bounded by the ensemble energy of the eigensubspace formed by the eigenstates $|\Psi_0\rangle$ and $|\Psi_1\rangle$ of $\hat{H}(\kappa^*)$. Note that $|\Psi_A\rangle$ and $|\Psi_B\rangle$ can be any state obtained from a rotation between $|\Psi_0\rangle$ and $|\Psi_1\rangle$. In order to force $|\Psi_A\rangle$ and $|\Psi_B\rangle$ to be equal to either $|\Psi_0\rangle$ and $|\Psi_1\rangle$, we perform an additional rotation on the quantum computer according to Refs. [7, 51].

B. Optimization Methods

For the analysis in this paper, six optimization methods were selected based on their different properties so that a complete analysis could be performed.

The gradient-based optimization methods are employed, specifically Broyden-Fletcher-Goldfarb-Shanno method (BFGS) [67] and Sequential Least Squares Quadratic Programming (SLSQP) [68]. These gradient-based methods use derivatives to construct the step size and the step direction, and while they are usually efficient on smooth objective functions and fast in local convergence [69], they are usually not the best choice in a noisy environment [70, 71]. Yet, they are used in our calculations to provide an insight into how the specific noise types affect the landscape and the gradient calculations. BFGS is a quasi-Newton optimization method that uses an approximation of the Hessian matrix in each iteration, thus avoiding the direct calculation of costly second derivatives, and is particularly effective for medium-sized problems [72]. While in SLSQP the optimized problem is approximated as a quadratic programming problem, which is solved to update the overall best solution.

In the next subgroup, we have three gradient-free methods, namely Nelder-Mead Simplex method (NM) [73], Powell's method (PM) [74], and Constrained Optimization BY Linear Approximations (COBYLA) [75]. This group was chosen to investigate whether, when the need to calculate gradients is removed, better convergence can be achieved in an environment where quantum decoherence is present. The NM method in n -dimensional search space uses an $n + 1$ -dimensional simplex, which is iteratively updated using reflection, expansion, contraction, and shrinkage operations to search for the optimum. It is simple and efficient in lower dimensions, but convergence may worsen when the problem's dimensionality increases [76]. On the other hand, PM performs sequential line minimizations along a set of directions. These directions are later updated to improve conjugacy, thus speeding up the convergence. Usually, it works best on smooth problems and can stagnate in non-ideal conditions [77]. The last method of this set is COBYLA, a trust-region method that builds an approximation of both the objective function and constraints. Updates are performed within a region around the current point, which shrinks or expands adaptively [78].

The last investigated method is an example from global optimizers, specifically the Improved Self-Organizing Migrating Algorithm (iSOMA) [79, 80]. Global methods oftentimes use stochastic approaches and a population of candidate solutions to search for global optima. iSOMA's candidate solutions migrate toward the best-performing solution with adaptive step lengths, balancing exploration and exploitation, making it effective for global optimization of complex, multimodal landscapes [81]. Further details for the optimization methods are described in Section A.

C. Estimators

To examine the performance under noisy conditions, we first needed a benchmark; for this, a noiseless estima-

tor was configured, so that we could test the optimization method without the influence of inherent stochasticity or any decoherence. Meaning that the performance of the optimization method was tested on the base problem, without any influence of decoherence, which stems from quantum mechanics. The next step was to add the stochasticity. For this, we used four estimators, where the effect of finite sampling was included; the number of measurements for these estimators was set to four levels,

$$n_m \in \{256, 512, 1024, 6144\}. \quad (3)$$

This setting will allow us to quantify how the number of measurements influences the optimization process and the convergence.

Beyond sampling noise, we constructed a variety of realistic noise models using Qiskit Aer's `Estimator` [82].

Three decoherence channels from Qiskit Aer [83] were used: phase damping, depolarizing, and thermal relaxation. The phase-damping channel is defined as

$$\mathcal{E}_{\text{PD}}(\rho) = E_0 \rho E_0^\dagger + E_1 \rho E_1^\dagger, \quad (4)$$

with

$$E_0 = \begin{bmatrix} 1 & 0 \\ 0 & \sqrt{1-\lambda} \end{bmatrix}, \quad E_1 = \begin{bmatrix} 0 & 0 \\ 0 & \sqrt{\lambda} \end{bmatrix}, \quad (5)$$

where λ is the dephasing probability [84]. The depolarizing channel is given by

$$\mathcal{E}_{\text{Depol}}(\rho) = (1-p)\rho + \frac{p}{d}I, \quad (6)$$

where p is the depolarizing probability and d is the Hilbert-space dimension [85]. Finally, the thermal relaxation channel is expressed as

$$\mathcal{E}_{\text{TR}}(\rho) = \sum_{i=0}^2 E_i \rho E_i^\dagger, \quad (7)$$

where E_i depend on the gate duration t_g and relaxation times T_1 and T_2 [86].

All noise types were tested with multiple levels of error rates to encompass near-ideal, realistic, and really noisy conditions. For these calculations, the number of measurements was set to 6144 to minimize the role of stochasticity, as that was investigated independently.

Phase damping was applied with the following rates

$$r_{\text{PD}} \in \{1\%, 5\%, 10\%, 20\%\}, \quad (8)$$

which affected the R_z rotation gates. The depolarizing channel affecting the following single-qubit, $x, y, z, h, r_x, r_y, r_z$, and two-qubit cx gates, was simulated with the rates equaling to

$$r_{\text{Depol}} \in \{1\%, 5\%, 10\%, 20\%\}. \quad (9)$$

As we also wanted to test thermal relaxation conditions, two distinct sets were investigated. The first one, which

mimics realistic conditions, has relatively long T_1 and T_2 times. Here we varied the T_2 time as follows

$$T_2 \in \{70, 80, 180, 380\} \mu\text{s}, \quad (10)$$

and setting $T_1 = T_2 + 20\mu\text{s}$. The intention of the second set was to look at shorter relaxation times, where

$$T_2 \in \{50, 100, 200, 300\} \text{ ns}, \quad (11)$$

and $T_1 = T_2$. For both of the sets examining thermal relaxation, realistic gate durations of 50 ns for single-qubit and 150 ns for two-qubit operations were set. Together, these two types of models capture both extended coherence and rapid decay conditions, allowing us to examine the optimization methods' abilities under varying conditions.

II. RESULTS

To evaluate the effect of different types of noise described in Section IC, on the performance of SA-OO-VQE, we focus on the six methods described in Section IB.

A. Accuracy of Results

At first, the accuracy was investigated. As SA-OO-VQE is able to calculate both ground and excited states, the results are visualized in Figure 1. In these scatter plots, the x-axis represents the energy of the ground state, the y-axis corresponds to the excited state energy, and the dashed lines show the optimal solution. Different noise types are represented by distinct markers.

It can be seen that SLSQP, visualized in Figure 1(a), fails to converge correctly even with just stochastic noise, and the problems only get worse when different noise types are considered. The spread of outcomes of different runs with the same noise is also large. iSOMA, shown in Figure 1(b), also shows some degree of spread, for it is significantly smaller than in the SLSQP case. The solutions for stochastic noise are clustered around the optimized value; this is, in a way, an expected behaviour as iSOMA is a global optimizer, and some kind of variance, around the optimal value is expected.

If we have a look at PM, Figure 1(c), NM, Figure 1(d), and COBYLA, Figure 1(e) we can observe similar behaviour for these three optimizers. They tend to cluster relatively well, for each type of noise, and also, we can see that if the rate of noise is increased for the same noise type, the results are worse, which agrees with the expected behaviour. The best results, at least from the point of optimized energies, were obtained via BFGS, Figure 1(f). Here we see well-defined clusters, with expected behaviour.

To establish a baseline for all noise models, let us have a look at ideal, noiseless conditions first. Under these

idealized conditions, the results shown in Table I, tell us an expected results, as all local optimizer managed to converge to the energy value $\mu_{\text{Final}} = 1.124053$, which is the optimal state-averaged energy, whose ground and excited state components correspond to the reference values obtained via Psi4 [87]. The notable difference is in the mean number of evaluations, μ_{Evals} , that were necessary to achieve convergence. Here we can see that both BFGS and SLSQP are the best performing optimizers, taking tens of evaluations to converge, thus being the most efficient optimizers, with BFGS taking a slight lead. It is also important to note that the $\sigma_{\text{Evals}} < 15$, which is the standard deviation, for both of the optimizers, making sure that even in the worst-case, the optimizer did not require a significantly larger amount of function evaluations. The other local optimizers needed hundreds of function evaluations to converge, and the σ_{Evals} was also proportionally larger. The third best optimization method for ideal conditions is NM, followed by PM and then COBYLA. What was expected is that the global optimizer, iSOMA, would have the hardest time reaching the minimum, ending with over a thousand function evaluations and unable to, on average, achieve the global optimum. The high number of function evaluations is due to the population-based core of the algorithm, and the non-optimal value of energy shows us that in the ideal condition and in the case of a small system like H_2 , it is unnecessary to employ a sophisticated global optimizer as the search space's dimensionality is low, and there are no distortions that would require such method.

With the noiseless baseline established, the focus turns to the first kind of noise, which is inherent for all calculations performed on quantum computers, and that is the sampling noise, which stems from the inherent stochasticity of quantum mechanics. The presence of sampling noise, data shown in Table II, in the optimization process does not prevent most optimizers from attaining the ideal state-average energy, but the accuracy is lower than in the case of ideal conditions. Gradient-based BFGS consistently reaches within 10^{-3} of the desired value, while keeping the number of iterations in the hundreds. This number also decreases with the increase of measurements, showing a trend that we can achieve faster convergence with a slightly higher number of measurements. This makes BFGS highly efficient. Deterministic derivative-free methods, NM and PM, also show the ability to achieve near-perfect final energy, but the number of function evaluations is notably higher than for BFGS. For iSOMA and COBYLA, the results are quite similar, but COBYLA requires about ten times fewer function evaluations, making it the optimizer with the fewest evaluations required. The one method that failed in all cases is SLSQP, as it was unable to achieve the optimum and still required a high number of evaluations.

So overall, BFGS proves to be a quick and reliable choice, followed by COBYLA if we need good enough results and low computational cost, or PM and if we want better accuracy, which comes with 3–4 times higher com-

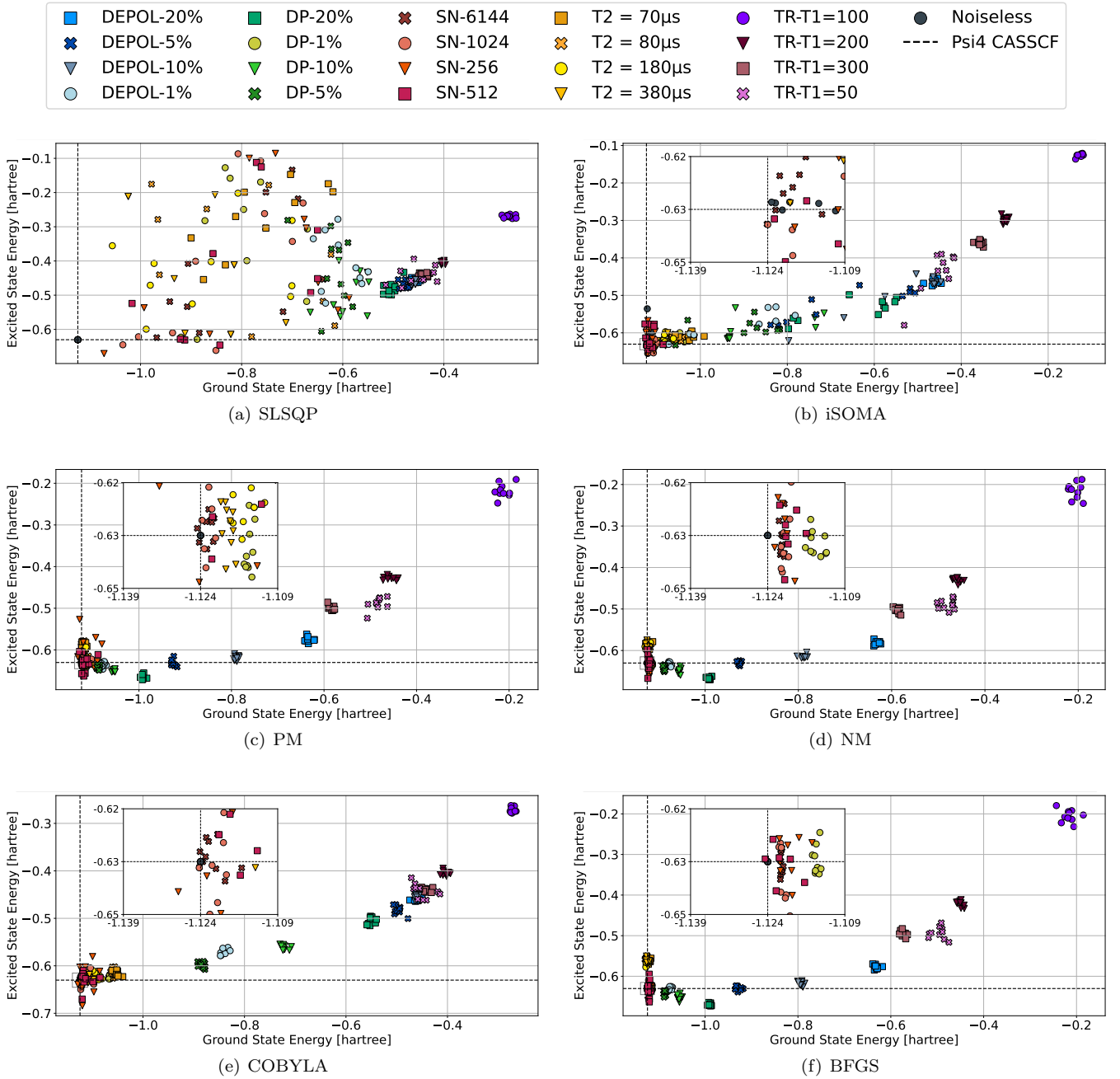


FIG. 1. Scatter plots of ground state energy (x-axis) and excited state energy (y-axis) for each optimization method. Dashed lines indicate the ideal values. All noise models are shown. The shared legend is displayed once at the top and removed from individual panels.

putational cost. While NM achieves good results in terms of accuracy, the number of evaluations it requires lets it be outperformed by other methods. Even the global optimizer, iSOMA, needs about half the iterations to grant comparable results.

Moving on to the models containing decoherence. The first results depicting different levels of dephasing noise are shown in Table III. The introduction of dephasing noise into our model leads to systematic worsening of

our results. For the 1% level of noise, BFGS, NM, and PM perform relatively well with COBYLA and iSOMA coming in the second tier, whereas SLSQP has significant convergence problems even in the lowest noise levels, rendering it unusable. With the increasing dephasing noise levels, the performance of the optimizers worsens, while the number of function evaluations remains similar, telling us that the dephasing noise distorts the landscape evenly without creating any new difficulties.

What is interesting is the fact that for NM, higher levels of noise lead to a decrease in evaluations that are necessary while having results comparable to BFGS and PM. This tells us that for NM, the distortions of the landscape made by dephasing noise lead to faster convergence, probably because the inherent changes make the optimizer stay longer with larger differences in chosen coordinates. Overall, we see that fine results are achieved under 1% noise, and the absolute error is increasing linearly with the noise.

In the case of depolarizing noise, we can observe higher levels of deviations than in the case of dephasing noise. This is visualized in Table IV. The best overall performer is BFGS, leading both in the best energy and a fairly low number of iterations as opposed to NM and PM, where the number of evaluations is in thousands. In this type of noise, we see COBYLA failing, and along with SLSQP being the most affected by the noise. iSOMA is showing similar behavior as in previous cases, that is, having trouble finding the optimal values.

Moving on to the case of thermal relaxation under feasible conditions that are similar to those on current quantum computers. From Table V we observe the fact that BFGS is consistently the top performer. This shows that in small search spaces, this method is resistant to thermal relaxation, and also is the fastest converging method. On the other hand, SLSQP is consistently the worst, performance-based, as it has trouble even in the longest relaxation time. The other two methods we can say are not a viable choice are NM and iSOMA, because the number of evaluations is significantly higher, and thus this makes them inefficient. The last examined method is PM, where the results did not linearly correlate with the thermal relaxation level; thus, it is a choice that is unreliable, as with the scaling of the thermal relaxation, we do not get improvement in the expected direction.

The last set of estimators, with unrealistic times of thermal relaxation, [88] is displayed in Table VI. These numbers display several things, firstly, that under these noise levels, there is no way for any algorithm to converge, as with these times, the information encoded into the ansatz vanishes, this is the effect known as noise limit, as even with the largest relaxation time, only the last few gates that are applied have any reasonable chance to affect the calculations. While there still remains variance in terms of the number of function evaluations, the expected behavior is displayed, as the results have a tendency to cluster in the same region, around similar values. This shows that these levels of noise are the only dominant factor, and that the choice of the optimization method itself is not significant, as it has a minor influence, and the obtained results are unusable.

Also, an additional analysis was done with respect to the unrealistic T_2 and T_1 values, to better understand how the method behaves near its noise limit. The values themselves were chosen to reflect the range all the way to 0.1 ns. It is shown in Figure 2. This was done only with BFGS optimization method and the values were scaled all

Optimizer	μ_{Final}	σ_{Final}	μ_{Evals}	σ_{Evals}
BFGS	-1.124053	0.000000	37.10	9.80
COBYLA	-1.124051	0.000004	433.60	70.52
iSOMA	-1.115658	0.008464	1135.80	366.53
NM	-1.124053	0.000000	295.20	25.27
PM	-1.124053	0.000000	396.00	33.38
SLSQP	-1.124053	0.000000	52.00	12.65

TABLE I. Summary of optimization results under ideal conditions.

Optimizer	μ_{Final}	σ_{Final}	μ_{Evals}	σ_{Evals}
SN-256				
BFGS	-1.120850	0.001351	363.10	190.07
COBYLA	-1.112210	0.021526	286.70	54.63
iSOMA	-1.113026	0.010187	2040.40	393.25
NM	-1.121963	0.001194	4787.10	827.51
PM	-1.104752	0.025028	988.40	172.07
SLSQP	-0.886073	0.157799	1608.10	325.35
SN-512				
BFGS	-1.121398	0.000759	365.50	134.29
COBYLA	-1.118548	0.008037	248.30	35.34
iSOMA	-1.114753	0.009960	2215.50	607.06
NM	-1.120785	0.000954	5082.40	1251.06
PM	-1.116395	0.009086	1027.10	212.34
SLSQP	-0.793686	0.173310	1527.30	336.02
SN-1024				
BFGS	-1.121119	0.000820	295.10	67.72
COBYLA	-1.114944	0.007365	270.60	50.13
iSOMA	-1.113874	0.009434	1739.00	500.15
NM	-1.120932	0.000928	5179.90	569.66
PM	-1.120962	0.004637	837.00	182.30
SLSQP	-0.903307	0.172749	1674.30	280.76
SN-6144				
BFGS	-1.121203	0.000382	296.50	58.39
COBYLA	-1.122400	0.001345	254.40	32.49
iSOMA	-1.116929	0.011109	2037.50	749.76
NM	-1.121183	0.000428	5176.50	880.26
PM	-1.122546	0.002113	964.70	264.61
SLSQP	-0.782598	0.149267	1283.10	225.45

TABLE II. Summary of optimization results under sampling noise.

the way to 0.1. This shows that with large enough levels of noise, the results are converging to a value, which is mainly influenced by the Hamiltonian of the problem.

B. Statistical Analysis

To broaden the scope of the obtained results and to obtain the general findings as much as possible, an encompassing statistical analysis was done next. First, the analysis of the spread, i.e., how large the clusters are, and differences of the clusters created by different estimator settings was performed to see if there are indeed statistical differences between the individual clusters. This anal-

Optimizer	μ_{Final}	σ_{Final}	μ_{Evals}	σ_{Evals}
DP-1%				
BFGS	-1.114730	0.000635	335.70	59.57
COBYLA	-1.066868	0.002831	274.40	41.16
iSOMA	-1.043178	0.012105	2356.70	1096.66
NM	-1.114112	0.001037	4090.20	1887.48
PM	-1.114574	0.001005	1620.30	800.79
SLSQP	-0.807131	0.121553	1679.20	412.94
DP-5%				
BFGS	-1.087991	0.001559	347.80	85.84
COBYLA	-0.882381	0.007467	264.10	48.66
iSOMA	-0.890502	0.082490	2648.50	1176.03
NM	-1.086391	0.001657	2943.00	742.09
PM	-1.087121	0.001709	1305.00	384.04
SLSQP	-0.638770	0.047198	1315.20	231.53
DP-10%				
BFGS	-1.053551	0.002349	296.70	60.82
COBYLA	-0.714788	0.010197	260.60	39.63
iSOMA	-0.869096	0.100150	2081.40	645.04
NM	-1.054817	0.002169	3041.80	1059.16
PM	-1.054651	0.002056	1460.80	559.85
SLSQP	-0.585455	0.046439	1433.30	455.71
DP-20%				
BFGS	-0.993124	0.003935	334.10	83.85
COBYLA	-0.552636	0.008491	284.30	18.92
iSOMA	-0.642074	0.102140	1808.40	380.16
NM	-0.992108	0.002812	2737.40	829.93
PM	-0.993125	0.004564	1470.50	417.57
SLSQP	-0.500512	0.007260	1609.90	521.27

TABLE III. Summary of optimization results under dephasing noise models.

Optimizer	μ_{Final}	σ_{Final}	μ_{Evals}	σ_{Evals}
DEPOL-1%				
BFGS	-1.075892	0.001902	304.70	64.05
COBYLA	-0.842345	0.007302	285.20	65.42
iSOMA	-0.910764	0.107383	2103.40	639.58
NM	-1.075821	0.002196	2636.80	702.12
PM	-1.076834	0.002692	1435.10	305.30
SLSQP	-0.644954	0.044021	1274.10	183.04
DEPOL-5%				
BFGS	-0.926838	0.003819	415.70	123.57
COBYLA	-0.497159	0.006110	247.40	26.25
iSOMA	-0.662891	0.139207	2432.30	987.37
NM	-0.926605	0.004067	2640.40	701.85
PM	-0.927095	0.002709	1725.00	520.84
SLSQP	-0.478193	0.008645	1266.20	230.18
DEPOL-10%				
BFGS	-0.794687	0.005111	337.00	81.42
COBYLA	-0.463104	0.003334	236.00	23.67
iSOMA	-0.529579	0.116088	2281.30	572.57
NM	-0.791182	0.003995	2843.70	1138.18
PM	-0.792864	0.005558	1823.60	657.97
SLSQP	-0.461766	0.005858	1304.40	222.70
DEPOL-20%				
BFGS	-0.630411	0.001677	316.40	58.63
COBYLA	-0.460570	0.004747	282.00	43.91
iSOMA	-0.464260	0.006281	2110.40	529.50
NM	-0.633490	0.004929	2943.10	739.55
PM	-0.629442	0.005980	1369.70	374.21
SLSQP	-0.460514	0.007062	1370.10	229.13

TABLE IV. Summary of optimization results under depolarizing noise models.

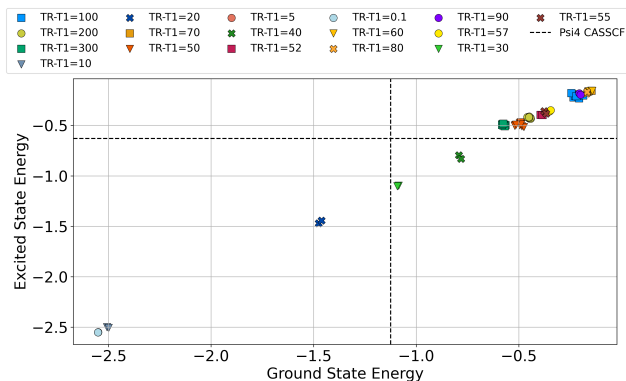


FIG. 2. Further analysis and scaling of unrealistic T_1 and T_2 values.

ysis was performed for every optimizer independently to examine how the different types of decoherence affect the results of the optimization process.

Next, we focused on the comparison of the optimizers themselves, first in a setting-by-setting manner, where the comparison is between distinct optimization methods, while keeping the conditions the same. Eventually, we investigated at the overall ranking of the methods, with respect to the chemical accuracy, as that is the

most important aspect when running chemical calculations. A brief additional analysis regarding the number of cost function evaluations was also performed, further supporting the results and strengthening the overall conclusions of this study.

In the first parts of the statistical analysis, the goal was to determine whether the clusters for different estimators are significantly different in the position of centroids or not, to better judge if all noises affect the optimization process distinctly. For this, we have chosen a per optimization method approach, so that the effect of the decoherence could be studied independently.

At first, a Multivariate Analysis of Variance (MANOVA) [89, 90] was chosen to determine if there are statistically significant differences with respect to the position of centroids between the clusters of data all at once.

The suitability of MANOVA was evaluated through a series of assumption checks, the full details of which are reported in Section B. In brief, tests of multivariate normality and homogeneity of covariance structures (including Mardia's test, Box's M , Levene's, and Brown-Forsythe procedures) consistently indicated significant deviations from the required conditions. In particular, the equality of covariance matrices and variances across

Optimizer	μ_{Final}	σ_{Final}	μ_{Evals}	σ_{Evals}
T2 = 70μs				
BFGS	-1.122428	0.002691	293.70	54.20
COBYLA	-1.055532	0.003830	445.50	56.68
iSOMA	-1.029268	0.018616	1953.80	399.60
NM	-1.120829	0.003170	3047.40	1063.07
PM	-1.117958	0.003686	1367.40	344.32
SLSQP	-0.762712	0.098260	751.80	246.60
T2 = 80μs				
BFGS	-1.122921	0.003397	324.90	84.45
COBYLA	-1.059595	0.005007	422.10	63.62
iSOMA	-1.061441	0.028576	1965.60	548.02
NM	-1.121465	0.002912	2743.90	1066.15
PM	-1.115830	0.004948	1085.30	224.42
SLSQP	-0.790968	0.144783	645.20	175.81
T2 = 180μs				
BFGS	-1.123770	0.003853	369.50	105.66
COBYLA	-1.091851	0.005649	387.80	69.27
iSOMA	-1.079421	0.005654	1888.70	398.09
NM	-1.122740	0.003461	3047.70	1062.96
PM	-1.084546	0.101001	765.40	337.73
SLSQP	-0.865482	0.135434	797.40	208.41
T2 = 380μs				
BFGS	-1.125712	0.005031	329.50	86.37
COBYLA	-1.103739	0.009152	299.20	34.36
iSOMA	-1.098443	0.013342	2586.10	818.29
NM	-1.124246	0.003378	2745.90	828.78
PM	-1.118999	0.000687	351.70	212.30
SLSQP	-0.808040	0.195677	794.50	255.29

TABLE V. Summary of optimization results under T_2 noise models mimicking realistic conditions.

noise settings was systematically violated, demonstrating that the data exhibit heterogeneous dispersion and non-Gaussian structure. These results indicate that the parametric assumptions underlying MANOVA are not satisfied for the present dataset.

So instead, we adopted the Permutational Multivariate Analysis of Variance (PERMANOVA) [91] to help us figure out if there are statistically significant differences in the individual clusters, as PERMANOVA is a non-parametric method that partitions variation in a distance matrix among groups and assesses significance using permutations. It does not assume multivariate normality but relies on the assumption of independent observations.

The assumption of independent observations is met by the design of how these results were obtained. But let us have a look at the multivariate dispersions, so that we can interpret the PERMANOVA results more clearly, when we present them.

For this, the Permutational Analysis of Multivariate Dispersions (PERMDISP) [92] approach was chosen. In this procedure, the distance of each observation to its group centroid in multivariate space is computed, and these distances are then subjected to a one-way Analysis of variance (ANOVA) [93]. The details of this approach and the analysis results themselves are discussed in detail

Optimizer	μ_{Final}	σ_{Final}	μ_{Evals}	σ_{Evals}
TR-T1 = 50				
BFGS	-0.491281	0.015304	392.70	104.28
COBYLA	-0.438886	0.014340	433.60	114.71
iSOMA	-0.452341	0.056327	2336.40	581.44
NM	-0.493719	0.009967	3079.60	1270.86
PM	-0.505781	0.010593	1456.10	386.38
SLSQP	-0.437642	0.025683	1821.00	313.57
TR-T1 = 100				
BFGS	-0.211467	0.017875	473.90	140.48
COBYLA	-0.267755	0.005440	285.30	56.76
iSOMA	-0.127668	0.007830	1916.10	548.77
NM	-0.216100	0.015541	3008.40	900.78
PM	-0.220340	0.012304	1989.30	886.94
SLSQP	-0.267370	0.003906	1865.70	426.46
TR-T1 = 200				
BFGS	-0.446706	0.007617	354.20	71.42
COBYLA	-0.395097	0.007213	301.70	44.36
iSOMA	-0.298103	0.005032	2139.70	524.19
NM	-0.460963	0.006728	2863.50	797.29
PM	-0.462090	0.004899	1753.80	325.92
SLSQP	-0.400840	0.004440	1335.89	292.10
TR-T1 = 300				
BFGS	-0.571573	0.004647	402.40	111.41
COBYLA	-0.442324	0.008752	282.40	77.91
iSOMA	-0.354515	0.006189	2207.70	792.10
NM	-0.587468	0.005057	2852.80	926.76
PM	-0.586655	0.007705	1696.00	264.08
SLSQP	-0.435964	0.006146	744.40	251.22

TABLE VI. Summary of optimization results under **TR-T1** noise models to test unrealistic conditions.

in Section C.

The detailed analysis is described in Section D, but we can say that overall, the pairwise post hoc analyses show a pretty consistent pattern across all of the optimization methods. For most of the pairs, there is a significant difference in both the location of the centroid and in the dispersion. The pairs that are statistically not different mostly consist of sampling noise, low levels of dephasing channel, and some categories of T_2 .

C. Bootstrapping

Next, we wanted to gain more insight about the results of the optimization methods, so we turned to Bootstrapping 95% predictions for all optimizers in the ground vs excited energy plane, with the goal to be able to concretely predict the optimization outcomes for all methods and settings. This means that out of 100 samples, 95 of them will be in our defined area.

We visualize each family with a 95% predictive ellipse in the (x, y) plane, defined as the set of points whose squared Mahalanobis distance [94] to the group mean μ (with covariance Σ) does not exceed a bootstrap-

estimated cutoff $d_{0.95}^2$,

$$\mathcal{E}_{0.95} = \{ \mathbf{x} \in \mathbb{R}^2 : (\mathbf{x} - \boldsymbol{\mu})^\top \boldsymbol{\Sigma}^{-1} (\mathbf{x} - \boldsymbol{\mu}) \leq d_{0.95}^2 \}. \quad (12)$$

For each family, $\boldsymbol{\mu}$ and $\boldsymbol{\Sigma}$ are computed from its points, then $d_{0.95}^2$ is obtained by bootstrap resampling of the group, taking within-bootstrap 95th percentiles of Mahalanobis distances and using their median across bootstraps. The ellipse center indicates location (group mean), its area reflects within-group dispersion, and its tilt encodes covariance structure. The separation of centers suggests location differences, while differing sizes or overlaps highlight dispersion heterogeneity, complementing the formal PERMANOVA and PERMDISP results.

The ellipses are visualized in Figure 3. In these figures, we observe several things, firstly, that for reasonable noise levels SLSQP, Figure 3(a), is widely spread, showing that the obtained results will not be clustered, so this method is not really a good choice if we desire consistent results. The global optimizer iSOMA, Figure 3(b), is compared to SLSQP, which is more clustered, but due to its heuristic nature, it is still outperformed by PM, Figure 3(c), NM, Figure 3(d), BFGS, Figure 3(f), and COBYLA, Figure 3(e).

For the last four mentioned optimizers, we see tighter clusters, pointing to the fact that these methods are under the same conditions clustering to the same value, showing that we are getting consistent values, and that each of the runs is well representative of the behavior of the optimizer.

This concludes the intra-optimizer analysis of the runs, and we can now move to the comparison of different optimization methods' performance.

D. Overall Comparison

To begin with, the overall performance of the optimizers was compared. This was done by comparing their relative accuracy with respect to the Psi4 reference values, obtained by running Complete Active Space Self-Consistent Field (CASSCF). This is shown in Table VII, where the overall mean and root-mean-square (RMS) distance which is calculated as

$$\text{RMS} = \sqrt{\frac{1}{n} \sum_{i=1}^n (x_i - x_i^{\text{ref}})^2} \quad (13)$$

where x_i denotes the computed value for the i -th data point, x_i^{ref} is the corresponding reference value obtained from CASSCF using Psi4, and n is the total number of data points. The average rank across categories with its standard deviation (SD), and the number of categories and total data points used in the calculation, are shown. There we can observe that PM achieved the lowest overall mean error equaling to 0.209, and it was closely followed by NM at 0.211, and BFGS with a value of 0.216, while the worst performance is associated with SLSQP, with a

TABLE VII. Overall optimizer performance. Lower values of mean and RMS distance indicate better agreement with the Psi4 reference. Ranks are average \pm SD across 21 categories.

Optimizer	Mean	RMS	Avg. Rank	SD	Cat.	Points
PM	0.209	0.355	2.36	1.22	21	210
NM	0.211	0.356	2.10	1.09	21	210
BFGS	0.216	0.357	2.64	1.33	21	210
iSOMA	0.328	0.473	4.57	0.93	21	210
COBYLA	0.329	0.460	3.90	1.41	21	210
SLSQP	0.523	0.559	5.43	1.25	21	210

TABLE VIII. Global Friedman test of optimizer differences. The test was conducted across 21 categories common to all six optimizers.

k (methods)	n (blocks)	χ^2	p -value	Kendall's W
6	21	54.35	1.8×10^{-10}	0.518

value of 0.523, and iSOMA with COBYLA were constant under-performers with respect to the best three methods.

The global Friedman's test [95], with the null hypothesis defined as

$$H_0 : \bar{R}_1 = \bar{R}_2 = \dots = \bar{R}_k \quad (14)$$

where \bar{R}_j is the mean rank of optimizer j across n categories and k is the number of optimizers, confirmed that optimizer choice had a strong effect, with the values displayed in Table VIII, and are indicative of a moderate-to-strong effect across the 21 categories. To explain further, the Friedman test evaluates whether the rankings of optimizers differ across blocks (categories), while Kendall's W [96, 97], with the null hypothesis equaling to

$$H_0 : W = 0 \quad (15)$$

where $W \in [0, 1]$ is Kendall's coefficient of concordance over the rank matrices, provides an effect size, ranging from 0, meaning no agreement in rankings, to 1, signaling perfect agreement. Kendall's coefficient of concordance W is computed as

$$W = \frac{12S}{k^2(n^3 - n)} \quad (16)$$

where $S = \sum_{j=1}^k (\bar{R}_j - \frac{n+1}{2})^2$, k is the number of optimizers, n is the number of categories (blocks), and \bar{R}_j is the sum of ranks assigned to optimizer j across all categories.

The observed value of $W = 0.518$ therefore reflects a moderate-to-strong agreement among categories. The Friedman's test is a valid choice here as it is suitable for repeated measurements of data, and the categories are treated as blocks in the test. Also, there is no assumption of normality, and we only need ordinal data and balanced block sizes, which we both have.

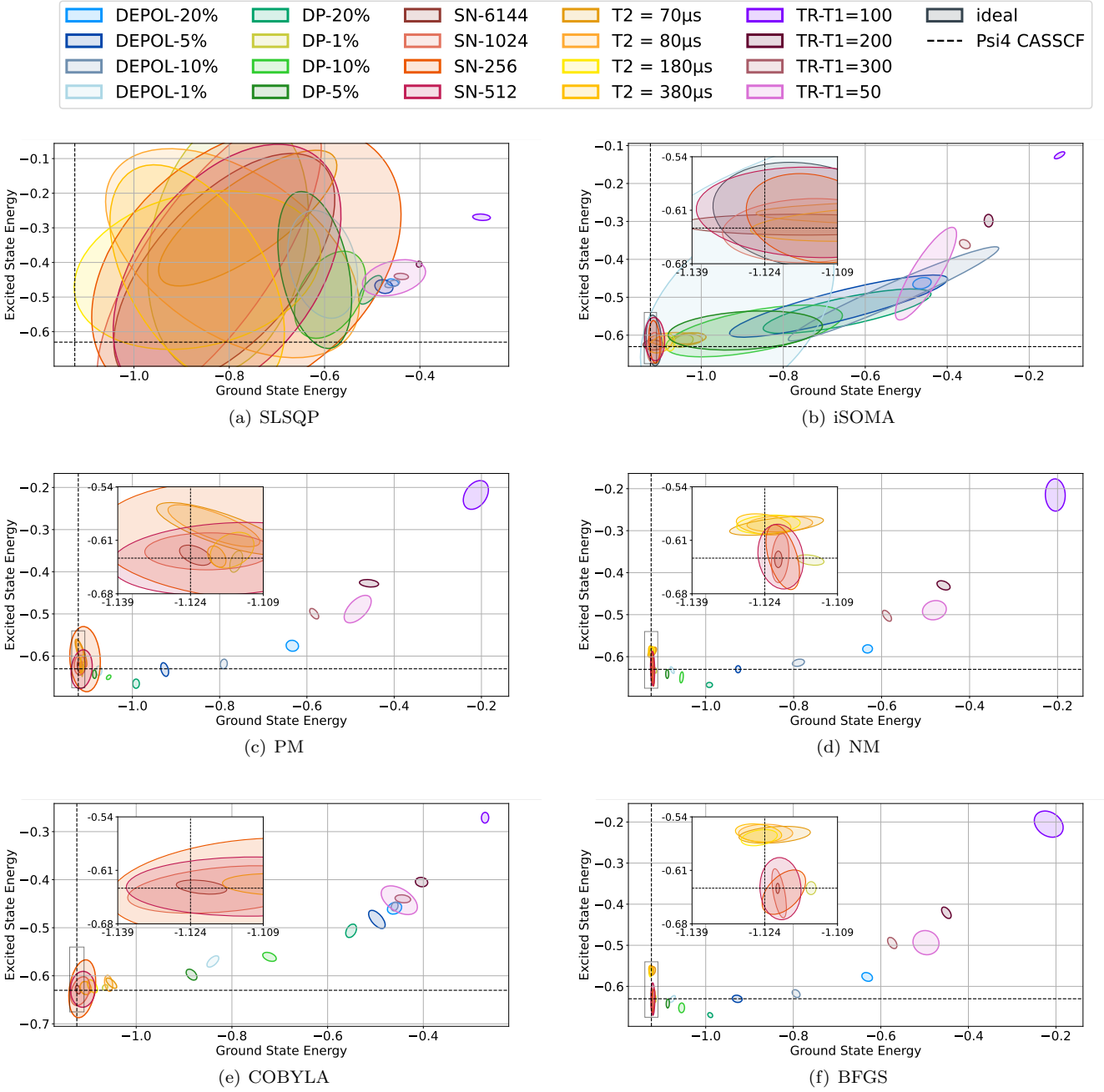


FIG. 3. Bootstrapped 95% prediction ellipses in the ground versus excited state energy plane for all optimization methods. Ellipses indicate the variability and orientation of results within families. Dashed lines mark the reference energies from Psi4 CASSCF.

Next, we have a look at the distribution of the mean distances from the Psi4 reference values and their associated 95% confidence intervals, which are illustrated in Figure 4. This type of visualization shows that PM, NM, and BFGS form a distinct group with similar error rates, while iSOMA and COBYLA follow behind with SLSQP being the worst one overall. The logarithmic scale is used to emphasize the magnitude of the errors and accurately visualize the difference between the best and the worst

performer.

Next, we want to further investigate if there are any significant differences in the optimizers, so we turn to the pairwise Wilcoxon signed-rank test [98], with the null hypothesis for comparing two optimizers defined as

$$H_0 : \tilde{\Delta} = 0 \quad (17)$$

where $\tilde{\Delta}$ is the median of paired differences between two optimizers.

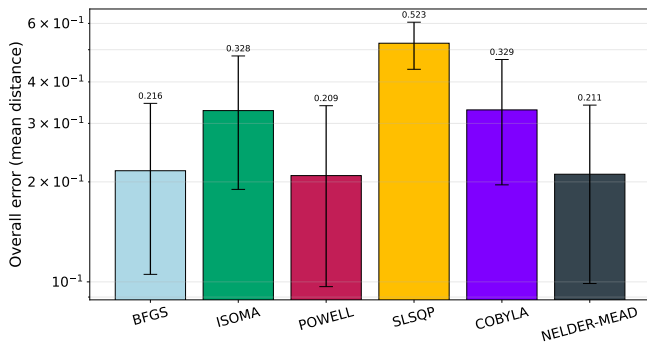


FIG. 4. Overall optimizer performance measured as mean distance to the Psi4 reference (bars $\pm 95\%$ bootstrap confidence interval on a log scale). Lower values indicate better agreement with the reference.

TABLE IX. Significant pairwise comparisons between optimizers based on Wilcoxon signed-rank tests across 21 categories. Reported are median paired differences (method_a – method_b) and Holm-adjusted p -values. Negative differences indicate that method_a performed better.

Comparison	Median diff.	W	p_{Holm}
PM vs SLSQP	-0.314	0.0	2.5×10^{-5}
NM vs SLSQP	-0.312	0.0	2.5×10^{-5}
BFGS vs SLSQP	-0.307	0.0	2.5×10^{-5}
COBYLA vs SLSQP	-0.195	0.0	4.2×10^{-4}
iSOMA vs SLSQP	-0.195	0.0	4.2×10^{-4}
PM vs iSOMA	-0.119	12.0	0.014
PM vs COBYLA	-0.118	12.0	0.014
NM vs iSOMA	-0.117	12.0	0.014
NM vs COBYLA	-0.116	12.0	0.014
BFGS vs iSOMA	-0.111	12.0	0.014
BFGS vs COBYLA	-0.110	12.0	0.014

The Holm correction [99] was also applied to control the family-wise error rate across all pairwise comparisons, as it provides stricter Type I error control than the Benjamini–Hochberg procedure, which is more suitable for exploratory analyses [100].

This test was performed on all 21 categories, and as it relies on paired comparisons between optimizers, it only assumes that the distribution of paired differences is symmetric around the median, and unlike parametric alternatives, it does not require normality of the data, so it is suitable for our case. Holm correction was chosen to control the family-wise error rate across all pairwise comparisons.

The results for this test are presented in Table IX, and they reveal that SLSQP was significantly worse than all other optimization methods, with p -values below the significance threshold of 0.05. In a similar manner, iSOMA and COBYLA were consistently outperformed by the other three methods, among which no significant difference was found any significant difference.

To focus on the problem with finer granularity and examine the differences within the individual noise cate-

gories. This is done because different types of noise may favor different optimization methods, and the good optimizer choice with respect to the known noise is crucial for obtaining the desired results.

For this, we plotted the grouped error for each optimization method, which is visible in Figure 5, and defined as the centroid distance to the Psi4 reference, which was computed as

$$D_{jc} = \sqrt{(\bar{E}_{g,jc} - E_g^{\text{ref}})^2 + (\bar{E}_{e,jc} - E_e^{\text{ref}})^2} \quad (18)$$

where D_{jc} denotes the centroid distance for optimizer j and noise type c , $\bar{E}_{g,jc}$ and $\bar{E}_{e,jc}$ are the mean ground and excited energies obtained for that optimizer–noise combination, and E_g^{ref} and E_e^{ref} are the corresponding Psi4 reference values.

There we see a direct comparison of the mean errors, for each configuration, where, as expected, for all methods except the SLSQP, the errors are significantly smaller in the ideal case, as SLSQP had convergence troubles even in the optimal case. Furthermore, we can observe how the error evolves with different levels of noise.

Next, across individual noise categories, tied-rank groupings derived from Friedman tests with Wilcoxon–Holm post-hoc comparisons showed consistent structure. The tied rankings were obtained by first applying the Friedman test within each noise setting to assess overall optimizer differences, followed by pairwise Wilcoxon signed-rank tests with Holm correction to identify significant contrasts. Optimizers that did not differ significantly at $\alpha = 0.05$ were grouped together by rank groups. This approach ensures that the reported ranks reflect statistically validated groupings rather than raw performance differences.

As displayed in the heatmap in Figure 6, in most categories, PM, NM, and BFGS occupied the top positions, often forming a statistically indistinguishable leading group, while SLSQP nearly always fell into the worst group. For example, in the SN-256 setting, BFGS and NM tied for best, with SLSQP uniquely last. In DP 1%, NM and BFGS dominated, with SLSQP again trailing. Under T_2 , PM emerged as the most stable method, taking sole first place at $180\mu\text{s}$ and $380\mu\text{s}$, whereas BFGS dropped markedly in these regimes. These tied rankings underline the heterogeneity across categories but also reinforce the general trend as the three quasi-Newton/simplex-type methods (PM, NM, BFGS) consistently populate the best statistical groups, iSOMA and COBYLA remain mid-field, and SLSQP is systematically the worst.

The optimizers were ranked by taking into account each pairwise rating and combining them into the ranked list. It was possible for multiple optimizers to share a rank, so the placement at the first placement meant that there had not been any statistical difference between the optimizers that rank in the same place, and all other optimizers were significantly worse. This process was done with all optimizers until all of them were assigned a place.

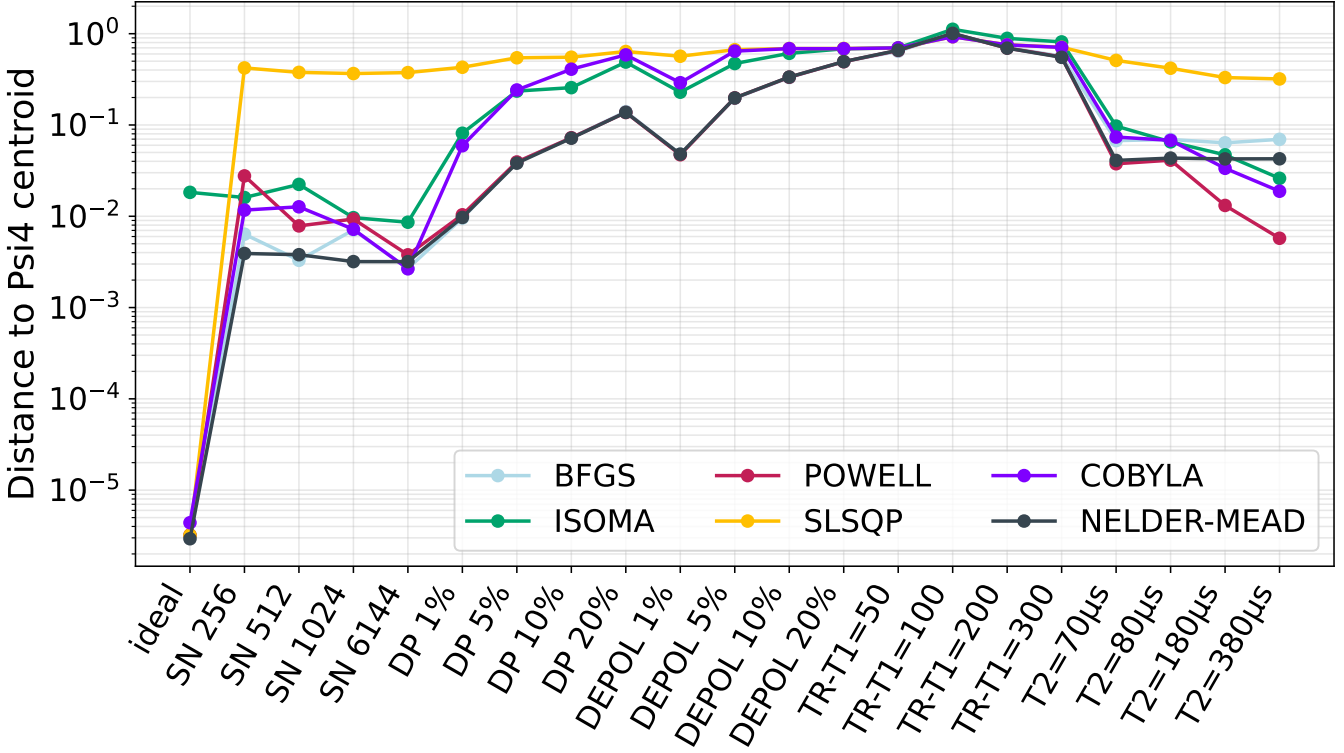


FIG. 5. Mean distance to the Psi4 reference for each optimizer across all noise categories. Lower values indicate better agreement with the reference.

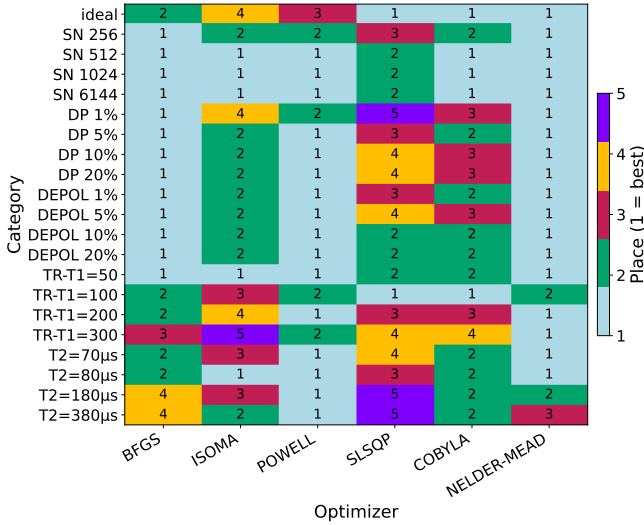


FIG. 6. Heatmap of optimizer ranks across noise categories. Darker shades indicate better ranks (1 = best). Each row corresponds to a category, and each column to an optimizer.

For further overview, the average place was calculated along with the number of placements in the best place, and this is all displayed in Table X.

Ranking analyses corroborated these conclusions. The Friedman test revealed a significant overall effect ($\chi^2 =$

TABLE X. Per-category rank summary of optimizers. Reported are the average place (1 = best), standard deviation (SD) of the rank across 21 categories, and the number of first-place finishes (#wins). Lower average place and more wins indicate more robust performance.

Optimizer	Avg. Place	SD	#Wins
NM	2.10	1.09	7
PM	2.36	1.22	6
BFGS	2.64	1.33	5
COBYLA	3.90	1.41	2
iSOMA	4.57	0.93	1
SLSQP	5.43	1.25	0

54.35, $p = 1.8 \times 10^{-10}$, Kendall's $W = 0.518$). Pairwise Wilcoxon tests with Holm correction further showed that BFGS, NM, and PM are statistically indistinguishable in performance, whereas SLSQP is significantly worse than all others ($p_{\text{Holm}} \leq 4.2 \times 10^{-4}$). COBYLA and iSOMA also underperformed relative to the top three optimizers, although their deficits were less severe.

The optimizers were quantitatively separated by the aggregated distance-to-reference metric. While COBYLA (0.329) and iSOMA (0.328) showed intermediate deviations from the exact reference, PM (0.209), NM (0.211), and BFGS (0.216) formed a high-performing cluster with small deviations. With the biggest dispar-

ity (0.523), SLSQP stood out and demonstrated its consistently subpar performance in every scenario that was tested.

III. SOFTWARE

All calculations in this work were obtained via the SA-OO-VQE software package [52], which is developed in Python and openly available at <https://gitlab.com/MartinBeseda/sa-oo-vqe-qiskit> and <https://pypi.org/project/saoovqe/>. The exact version of the solver used in this study corresponds to Git commit 504013abfe1b32a043a629295da003138aeeafa2, which is archived along with a replication package at Zenodo (DOI: 10.5281/zenodo.17296586) [101].

IV. CONCLUSIONS

The ideal conditions served as a benchmark, where all local optimizers converged, and only the global optimization method had trouble obtaining the correct results. The best method in this benchmark was BFGS, which showed extremely fast convergence. The global convergence method iSOMA did not provide any advantage, mainly due to the small dimensionality of the studied problem. And the outlook is that this method will become better suited when problems with higher dimensionality and with higher multimodality are studied.

In the case of sampling noise, where finite number of measurements was employed, convergence with adequate accuracy, 10^{-3} , is achievable, but new phenomena appears, and that is the fact that even due to this inherent noise, the variational principle, on which SA-OO-VQE method is build does not hold, and the obtained values can be lower than achieved energy. This can be mitigated with a sufficient number of measurements, but it still has to be considered. Also, in these conditions, BFGS, NM, and PM attained similar levels of accuracy, but from a pragmatic point of view, BFGS comes out the best as the other two methods required significantly higher numbers of function evaluations, thus being inefficient. One method that proved to be unreliable in all sampling noise levels was SLSQP, which failed to converge in all cases, and an increase in the number of measurements did not lead to an increase in accuracy.

Models with quantum decoherence showed a stronger influence on the results. When the dephasing channel was introduced, a slight but uniform decrease in accuracy arose, but the evaluation counts remained fairly stable. The same levels of depolarizing noise proved to have greater influence than their dephasing counterparts, but still BFGS remained the best, mainly due to its highest accuracy and stable and low number of evaluations. Next, in the case of realistic levels of thermal decoherence, the BFGS was the best performing, but the results were far from required accuracy, NM and iSOMA were

consistently inefficient, PM showed non-monotonic sensitivity to the noise, and SLSQP proved to be the worst choice. In the harsh conditions, where the times of thermal relaxations were by two orders of magnitude shorter than those found in current devices, it became apparent that the choice of the optimization methods becomes irrelevant, as there is nearly a full loss of information that is encoded in the ansatz.

The observed performance trends among the optimizers were further supported by statistical testing. The PERMANOVA analysis shown in Table XVII verified that the differences are highly significant ($p < 10^{-4}$ for all optimizers) and not anecdotal. Simultaneously, PERMDISP displayed in Table XVI showed dispersion heterogeneity, indicating that the observed variability is influenced by both centroid shifts and spread differences. These results show that distributional characteristics must be taken into account in order to fully capture optimizer performance, which cannot be achieved solely by averaging outcomes.

Mardia’s test of multivariate normality demonstrated that most optimizer-noise families retained approximate normality, with the notable exception of SLSQP in the ideal family. Specifically, significant deviations were detected in skewness ($p_{\text{skew}} = 0.002$) and kurtosis ($p_{\text{kurt}} = 0.041$). This highlights that optimizer instability can manifest even under noiseless conditions, underscoring the poor suitability of SLSQP for variational quantum eigensolver applications.

Comparing different noise types showed that, at equivalent nominal levels, depolarizing noise deteriorated results more than dephasing noise. For instance, BFGS maintained -1.0880 under 5% dephasing but converged to -0.9268 under 5% depolarization (Tables III and IV). Because sensitivity to noise is optimizer-dependent, this emphasizes how crucial it is to match optimizer strategies with the dominant error channels of particular quantum devices.

Interestingly, a counterintuitive trend was identified for NM under dephasing noise, where the number of required function evaluations decreased as noise increased (from 4090 at 1% to 2737 at 20%, Table III). This suggests that increased stochasticity may in some cases reshape the optimization landscape in ways that simplify convergence.

Finally, at extreme thermal relaxation limits (TR-T1 on the order of tens of ns), all optimizers converged to similarly poor energy values (Table VI). This demonstrates that under such conditions, the choice of optimizer becomes largely irrelevant compared to the hardware noise floor, as algorithmic improvements cannot compensate for the noise limit.

Overall, BFGS is consistently the best performer for small systems and SA-OO-VQE methods, where the combinations of accuracy and efficiency were shown. When there is the need to minimize the number of function evaluations, COBYLA proves to be the best choice if one is open to a slight decrease in accuracy ranging from 1% errors in stochastic noise to $< 6\%$ in the dephasing

time study, but the number of function evaluations stays under 500 in all the cases. On the other hand, one may look to NM or PM if the number of function evaluations is not an issue to have guaranteed higher levels of accuracy, as these methods were oftentimes among the best performers. iSOMA proves to be unnecessary for the low-dimensional problems, if the landscape does not exhibit pronounced multimodality. And the last examined method, SLSQP, constantly exhibits insufficient capabilities, rendering itself an ill choice for the investigated noisy environments.

In follow-up work, we will focus on two goals: one is the testing of different optimization models, specifically some that are designed for a noisy environment, so that better convergence can be attained consistently. Among these tested will be CMAES [102], BOBYQA [103], Bayesian optimization [104] and ADAM [105]. Although the present study highlights clear differences in optimizer performance, it remains unclear which specific features—such as population-based exploration, adaptive step-size control, or implicit regularization—are primarily responsible for improved noise resilience. Further investigation is required to determine how these properties interact with the structure of quantum noise and with the topology of the underlying energy landscape.

Secondly, the optimization methods must be tested on problems with higher dimensionality, where different molecules will be examined along with increases in active space. Here, it is not yet well understood how optimizer behavior scales with circuit depth, entanglement complexity, or the onset of barren plateaus. A systematic exploration of these factors will be essential for predict-

ing performance in large-scale quantum systems. Lastly, to efficiently test the performance of different optimizers on real-world quantum hardware, error mitigation techniques must be considered. At present, the coupling between specific mitigation schemes and optimizer dynamics is poorly characterized—particularly whether noise reduction strategies like zero-noise extrapolation or measurement mitigation affect convergence speed or bias differently across methods.

The final goal is to construct a guide where the best optimization method can be chosen based on a priori knowledge of the problem and noise structure. This guide will ultimately depend on bridging the remaining gaps in understanding between optimizer mechanisms, landscape geometry, and the stochastic nature of real quantum devices.

ACKNOWLEDGMENTS

Vojtěch Novák is supported by Grant of SGS No. SP2025/072, VSB-Technical University of Ostrava, Czech Republic. Martin Beseda was funded by Italian Government (Ministero dell’Università e della Ricerca, PRIN 2022 PNRR) – cod.P2022SELA7: ”RECHARGE: monitoRing, tEsting, and CHaracterization of performAnce Regressions“ – Decreto Direttoriale n. 1205 del 28/7/2023. This work was supported by the Ministry of Education, Youth and Sports of the Czech Republic through the e-INFRA CZ (ID:90254). This project has received funding from the Research Council of Lithuania (LMTLT), agreement No. P-ITP-24-9.

-
- [1] D. R. Simon, On the power of quantum computation, *SIAM Journal on Computing* **26**, 1474 (1997), <https://doi.org/10.1137/S0097539796298637>.
 - [2] A. W. Harrow, A. Hassidim, and S. Lloyd, Quantum algorithm for linear systems of equations, *Phys. Rev. Lett.* **103**, 150502 (2009).
 - [3] A. J. Daley, I. Bloch, C. Kokail, S. Flannigan, N. Pearson, M. Troyer, and P. Zoller, Practical quantum advantage in quantum simulation, *Nature* **607**, 667 (2022).
 - [4] Y. Cao, J. Romero, J. P. Olson, M. Degroote, P. D. Johnson, M. Kieferová, I. D. Kivlichan, T. Menke, B. Peropadre, N. P. Sawaya, *et al.*, Quantum chemistry in the age of quantum computing, *Chemical reviews* **119**, 10856 (2019).
 - [5] A. Rajamani, M. Beseda, B. Lasorne, and B. Senjean, How an equi-ensemble description systematically outperforms the weighted-ensemble variational quantum eigensolver (2025), arXiv:2509.17982 [quant-ph].
 - [6] S. Illésová, V. Novák, T. Bezděk, M. Beseda, and C. Possel, Numerical optimization strategies for the variational hamiltonian ansatz in noisy quantum environments, arXiv preprint arXiv:2505.22398 (2025).
 - [7] S. Illésová, M. Beseda, S. Yalouz, B. Lasorne, and B. Senjean, Transformation-free generation of a quasi-diabatic representation from the state-average orbital-optimized variational quantum eigensolver, *Journal of Chemical Theory and Computation* **21**, 5457 (2025), pMID: 40408769, <https://doi.org/10.1021/acs.jctc.5c00327>.
 - [8] T. Bezděk, H. Yuan, V. Novák, S. Illésová, and M. Beseda, Classical optimization strategies for variational quantum algorithms: A systematic study of noise effects and parameter efficiency, arXiv preprint arXiv:2511.09314 10.48550/arXiv.2511.09314 (2025).
 - [9] V. Novák, S. Illésová, T. Bezděk, I. Zelinka, and M. Beseda, Reliable optimization under noise in quantum variational algorithms, arXiv preprint arXiv:2511.08289 10.48550/arXiv.2511.08289 (2025).
 - [10] A. Di Meglio, K. Jansen, I. Tavernelli, C. Alexandrou, S. Arunachalam, C. W. Bauer, K. Borrás, S. Carrazza, A. Crippa, V. Croft, *et al.*, Quantum computing for high-energy physics: State of the art and challenges, *Prx quantum* **5**, 037001 (2024).
 - [11] C. Micheletti, P. Hauke, and P. Faccioli, Polymer physics by quantum computing, *Physical Review Letters* **127**, 080501 (2021).
 - [12] C. Ciaramelletti, M. Beseda, M. Consiglio, L. Lepori, T. J. G. Apollaro, and S. Paganelli, Detecting quaside-

- generate ground states in topological models via the variational quantum eigensolver, *Phys. Rev. A* **111**, 022437 (2025).
- [13] H. Lamm, S. Lawrence, Y. Yamauchi, and N. Collaboration, Parton physics on a quantum computer, *Physical Review Research* **2**, 013272 (2020).
- [14] P. Mocz and A. Szasz, Toward cosmological simulations of dark matter on quantum computers, *The Astrophysical Journal* **910**, 29 (2021).
- [15] Z. Guo, R. Li, X. He, J. Guo, and S. Ju, Harnessing quantum power: Revolutionizing materials design through advanced quantum computation, *Materials Genome Engineering Advances* **2**, e73 (2024).
- [16] N. P. De Leon, K. M. Itoh, D. Kim, K. K. Mehta, T. E. Northup, H. Paik, B. Palmer, N. Samarth, S. Sangtawesin, and D. W. Steuerman, Materials challenges and opportunities for quantum computing hardware, *Science* **372**, eabb2823 (2021).
- [17] S. Kang, Y. Kim, and J. Kim, Quantum computing based design of multivariate porous materials, *ACS Central Science* (2025).
- [18] X. Liu and M. C. Hersam, 2d materials for quantum information science, *Nature Reviews Materials* **4**, 669 (2019).
- [19] H. Ma, M. Govoni, and G. Galli, Quantum simulations of materials on near-term quantum computers, *npj Computational Materials* **6**, 85 (2020).
- [20] B. Bauer, S. Bravyi, M. Motta, and G. K.-L. Chan, Quantum algorithms for quantum chemistry and quantum materials science, *Chemical reviews* **120**, 12685 (2020).
- [21] A. Trovato, M. Beseda, and D. Di Nucci, A preliminary investigation on the usage of quantum approximate optimization algorithms for test case selection, in *Proceedings of the 2025 29th International Conference on Evaluation and Assessment in Software Engineering Companion*, EASE Companion '25 (Association for Computing Machinery, New York, NY, USA, 2025) p. 56–60.
- [22] M. Piattini, G. Peterssen, and R. Pérez-Castillo, Quantum computing: A new software engineering golden age, *ACM SIGSOFT Software Engineering Notes* **45**, 12 (2021).
- [23] S. Ali, T. Yue, and R. Abreu, When software engineering meets quantum computing, *Communications of the ACM* **65**, 84 (2022).
- [24] K. Dwivedi, M. Haghparast, and T. Mikkonen, Quantum software engineering and quantum software development lifecycle: a survey, *Cluster Computing* **27**, 7127 (2024).
- [25] A. K. Mandal, M. Nadim, C. K. Roy, B. Roy, and K. A. Schneider, Quantum software engineering and potential of quantum computing in software engineering research: a review, *Automated Software Engineering* **32**, 27 (2025).
- [26] M. De Stefano, F. Pecorelli, D. Di Nucci, F. Palomba, and A. De Lucia, Software engineering for quantum programming: How far are we?, *Journal of Systems and Software* **190**, 111326 (2022).
- [27] P. Lewandowska and M. Beseda, Benchmarking gate-based quantum devices via certification of qubit von neumann measurements, arXiv preprint arXiv:2506.03514 (2025).
- [28] A. B'ilek, J. Hlisenikovsk'y, T. Bezděk, R. Kukulski, and P. Lewandowska, Experimental study of multiple-shot unitary channels discrimination using the ibm q computers, *Scientific Reports* **16**, 6142 (2026).
- [29] T. Proctor, K. Young, A. D. Baczewski, and R. Blume-Kohout, Benchmarking quantum computers, *Nature Reviews Physics* **7**, 105 (2025).
- [30] T. Lubinski, S. Johri, P. Varosy, J. Coleman, L. Zhao, J. Necaie, C. H. Baldwin, K. Mayer, and T. Proctor, Application-oriented performance benchmarks for quantum computing, *IEEE Transactions on Quantum Engineering* **4**, 1 (2023).
- [31] A. Hashim, L. B. Nguyen, N. Goss, B. Marinelli, R. K. Naik, T. Chistolini, J. Hines, J. Marceaux, Y. Kim, P. Gokhale, *et al.*, Practical introduction to benchmarking and characterization of quantum computers, *PRX Quantum* **6**, 030202 (2025).
- [32] S. Illéssová, T. Rybotycki, and M. Beseda, Qmetric: Benchmarking quantum neural networks across circuits, features, and training dimensions, arXiv preprint arXiv:2506.23765 (2025).
- [33] V. Novák, I. Zelinka, and V. Snášel, Optimization strategies for variational quantum algorithms in noisy landscapes, arXiv preprint arXiv:2506.01715 (2025).
- [34] H. Yuan, C. K. Long, H. V. Lepage, and C. H. Barnes, Quantifying the advantages of applying quantum approximate algorithms to portfolio optimisation, arXiv preprint arXiv:2410.16265 (2024).
- [35] D. J. Egger, C. Gambella, J. Marecek, S. McFaddin, M. Mevissen, R. Raymond, A. Simonetto, S. Woerner, and E. Yndurain, Quantum computing for finance: State-of-the-art and future prospects, *IEEE Transactions on Quantum Engineering* **1**, 1 (2020).
- [36] P. Rebentrost, B. Gupt, and T. R. Bromley, Quantum computational finance: Monte carlo pricing of financial derivatives, *Physical Review A* **98**, 022321 (2018).
- [37] D. Herman, C. Googin, X. Liu, Y. Sun, A. Galda, I. Safro, M. Pistoia, and Y. Alexeev, Quantum computing for finance, *Nature Reviews Physics* **5**, 450 (2023).
- [38] R. Orús, S. Mugel, and E. Lizaso, Quantum computing for finance: Overview and prospects, *Reviews in Physics* **4**, 100028 (2019).
- [39] Y.-J. Chang, M.-F. Sie, S.-W. Liao, and C.-R. Chang, The prospects of quantum computing for quantitative finance and beyond, *IEEE Nanotechnology Magazine* **17**, 31 (2023).
- [40] M. K. Gupta, M. Beseda, and P. Gawron, How quantum computing-friendly multispectral data can be?, in *IGARSS 2022 - 2022 IEEE International Geoscience and Remote Sensing Symposium* (2022) pp. 4153–4156.
- [41] S. Illéssová, T. Rybotycki, P. Gawron, and M. Beseda, On the importance of fundamental properties in quantum-classical machine learning models, *International Journal of Parallel, Emergent and Distributed Systems* **0**, 1 (2026), <https://doi.org/10.1080/17445760.2026.2626759>.
- [42] V. Novák, I. Zelinka, L. Příbylová, L. Martínek, and V. Benčurik, Predicting post-surgical complications with quantum neural networks: A clinical study on anastomotic leak, arXiv preprint arXiv:2506.01708 (2025).
- [43] J. Biamonte, P. Wittek, N. Pancotti, P. Rebentrost, N. Wiebe, and S. Lloyd, Quantum machine learning, *Nature* **549**, 195 (2017).
- [44] S. Illéssová, T. Bezděk, V. Novák, I. Zelinka, S. Caccia-

- tore, and M. Beseda, From classical to hybrid: A practical framework for quantum-enhanced learning, arXiv preprint arXiv:2511.08205 10.48550/arXiv.2511.08205 (2025).
- [45] A. Aggarwal, S. V. Singh, S. Bansal, and V. Bhutani, A detailed overview of quantum computing machine learning techniques, in *2024 International Conference on Communication, Computer Sciences and Engineering (IC3SE)* (IEEE, 2024) pp. 1721–1725.
- [46] V. Novák, I. Zelinka, L. Příbylová, and L. Martínek, Quantum neural networks for propensity score estimation and survival analysis in observational biomedical studies, arXiv preprint arXiv:2506.19973 10.48550/arXiv.2506.19973 (2025).
- [47] S. Illéssová, E. Obeng, T. Bezděk, V. Novák, and M. Beseda, On the complementarity of classical classification and quantum neural networks in image classification, Preprints 10.20944/preprints202512.1348.v1 (2025), preprint.
- [48] J. Tilly, H. Chen, S. Cao, D. Picozzi, K. Setia, Y. Li, E. Grant, L. Wossnig, I. Rungger, G. H. Booth, *et al.*, The variational quantum eigensolver: a review of methods and best practices, *Physics Reports* **986**, 1 (2022).
- [49] D. A. Fedorov, B. Peng, N. Govind, and Y. Alexeev, Vqe method: a short survey and recent developments, *Materials Theory* **6**, 2 (2022).
- [50] S. Yalouz, B. Senjean, J. Günther, F. Buda, T. E. O’Brien, and L. Visscher, A state-averaged orbital-optimized hybrid quantum–classical algorithm for a democratic description of ground and excited states, *Quantum Sci. Technol.* **6**, 024004 (2021).
- [51] S. Yalouz, E. Koridon, B. Senjean, B. Lasorne, F. Buda, and L. Visscher, Analytical nonadiabatic couplings and gradients within the state-averaged orbital-optimized variational quantum eigensolver, *J. Chem. Theory Comput.* **18**, 776 (2022).
- [52] M. Beseda, S. Illéssová, S. Yalouz, and B. Senjean, State-averaged orbital-optimized vqe: A quantum algorithm for the democratic description of ground and excited electronic states, arXiv preprint arXiv:2401.11884 (2024).
- [53] H.-J. Werner and W. Meyer, A quadratically convergent mscf method for the simultaneous optimization of several states, *The Journal of Chemical Physics* **74**, 5794 (1981).
- [54] N. Moll, P. Barkoutsos, L. S. Bishop, J. M. Chow, A. Cross, D. J. Egger, S. Filipp, A. Fuhrer, J. M. Gambetta, M. Ganzhorn, *et al.*, Quantum optimization using variational algorithms on near-term quantum devices, *Quantum Science and Technology* **3**, 030503 (2018).
- [55] H. Qi, S. Xiao, Z. Liu, C. Gong, and A. Gani, Variational quantum algorithms: fundamental concepts, applications and challenges: H. qi et al., *Quantum Information Processing* **23**, 224 (2024).
- [56] G. S. Ravi, K. Smith, J. M. Baker, T. Kannan, N. Earnest, A. Javadi-Abhari, H. Hoffmann, and F. T. Chong, Navigating the dynamic noise landscape of variational quantum algorithms with qismet, in *Proceedings of the 28th ACM International Conference on Architectural Support for Programming Languages and Operating Systems, Volume 2* (2023) pp. 515–529.
- [57] P. Huembeli and A. Dauphin, Characterizing the loss landscape of variational quantum circuits, *Quantum Science & Technology* **6**, 025011 (2021).
- [58] E. Fontana, N. Fitzpatrick, D. M. Ramo, R. Duncan, and I. Rungger, Evaluating the noise resilience of variational quantum algorithms, *Physical Review A* **104**, 022403 (2021).
- [59] X. Ge, R.-B. Wu, and H. Rabitz, The optimization landscape of hybrid quantum–classical algorithms: From quantum control to nisq applications, *Annual Reviews in Control* **54**, 314 (2022).
- [60] B. Choy and D. J. Wales, Molecular energy landscapes of hardware-efficient ansätze in quantum computing, *Journal of chemical theory and computation* **19**, 1197 (2023).
- [61] A. K. Theophilou, The energy density functional formalism for excited states, *J. Phys. C: Solid State Phys.* **12**, 5419 (1979).
- [62] E. K. U. Gross, L. N. Oliveira, and W. Kohn, Rayleigh-ritz variational principle for ensembles of fractionally occupied states, *Phys. Rev. A* **37**, 2805 (1988).
- [63] K. M. Nakanishi, K. Mitarai, and K. Fujii, Subspace-search variational quantum eigensolver for excited states, *Phys. Rev. Res.* **1**, 033062 (2019).
- [64] M. Beseda, S. Illéssová, S. Yalouz, and B. Senjean, State-averaged orbital-optimized vqe: A quantum algorithm for the democratic description of ground and excited electronic states (1.2.0) (2025).
- [65] T. Helgaker, P. Jorgensen, and J. Olsen, *Molecular electronic-structure theory* (John Wiley & Sons, 2014).
- [66] J. Romero, R. Babbush, J. R. McClean, C. Hempel, P. J. Love, and A. Aspuru-Guzik, Strategies for quantum computing molecular energies using the unitary coupled cluster ansatz, *Quantum Sci. Technol.* **4**, 014008 (2018).
- [67] D. C. Liu and J. Nocedal, On the limited memory bfgs method for large scale optimization, *Mathematical programming* **45**, 503 (1989).
- [68] D. Kraft, A software package for sequential quadratic programming, *Forschungsbericht- Deutsche Forschungs- und Versuchsanstalt für Luft- und Raumfahrt* (1988).
- [69] M. S. Daoud, M. Shehab, H. M. Al-Mimi, L. Abualigah, R. A. Zitar, and M. K. Y. Shambour, Gradient-based optimizer (gbo): a review, theory, variants, and applications, *Archives of Computational Methods in Engineering* **30**, 2431 (2023).
- [70] G. Friedl and M. Kuczmann, Population and gradient based optimization techniques, a theoretical overview, *Acta Technica Jaurinensis* **7**, 378 (2014).
- [71] S. H. Haji and A. M. Abdulazeez, Comparison of optimization techniques based on gradient descent algorithm: A review, *PalArch’s Journal of Archaeology of Egypt/Egyptology* **18**, 2715 (2021).
- [72] Y.-H. Dai, Convergence properties of the bfgs algorithm, *SIAM Journal on Optimization* **13**, 693 (2002).
- [73] J. A. Nelder and R. Mead, A simplex method for function minimization, *The computer journal* **7**, 308 (1965).
- [74] M. J. Powell, An efficient method for finding the minimum of a function of several variables without calculating derivatives, *The computer journal* **7**, 155 (1964).
- [75] M. J. Powell, A direct search optimization method that models the objective and constraint functions by linear interpolation, in *Advances in optimization and numerical analysis* (Springer, 1994) pp. 51–67.
- [76] J. C. Lagarias, J. A. Reeds, M. H. Wright, and P. E. Wright, Convergence properties of the nelder–mead simplex method in low dimensions, *SIAM Journal on Opti-*

- mization **9**, 112 (1998).
- [77] B. Poljak, Nonlinear programming methods in the presence of noise, *Mathematical programming* **14**, 87 (1978).
- [78] A. Pellow-Jarman, I. Sinayskiy, A. Pillay, and F. Petrucione, A comparison of various classical optimizers for a variational quantum linear solver, *Quantum Information Processing* **20**, 202 (2021).
- [79] I. Zelinka, Soma—self-organizing migrating algorithm, in *Self-Organizing Migrating Algorithm: Methodology and Implementation* (Springer, 2016) pp. 3–49.
- [80] I. Zelinka, L. Kojecký, M. Lampart, J. Nowaková, and J. Plucar, isoma swarm intelligence algorithm in synthesis of quantum computing circuits, *Applied Soft Computing* **142**, 110350 (2023).
- [81] L. Klein, I. Zelinka, and D. Seidl, Optimizing parameters in swarm intelligence using reinforcement learning: An application of proximal policy optimization to the isoma algorithm, *Swarm and Evolutionary Computation* **85**, 101487 (2024).
- [82] https://qiskit.github.io/qiskit-aer/stubs/qiskit\protect_aer.primitives.Estimator.html.
- [83] https://qiskit.github.io/qiskit-aer/stubs/qiskit\protect_aer.noise.NoiseModel.html.
- [84] https://qiskit.github.io/qiskit-aer/stubs/qiskit\protect_aer.noise.PhaseDampingError.html.
- [85] https://qiskit.github.io/qiskit-aer/stubs/qiskit\protect_aer.noise.DepolarizingError.html.
- [86] https://qiskit.github.io/qiskit-aer/stubs/qiskit\protect_aer.noise.ThermalRelaxationError.html.
- [87] D. G. A. Smith, L. A. Burns, A. C. Simmonett, R. M. Parrish, M. C. Schieber, R. Galvelis, P. Kraus, H. Kruse, R. Di Remigio, A. Alenaizan, A. M. James, S. Lehtola, J. P. Misiewicz, M. Scheurer, R. A. Shaw, J. B. Schriber, Y. Xie, Z. L. Glick, D. A. Sirianni, J. S. O’Brien, J. M. Waldrop, A. Kumar, E. G. Hohenstein, B. P. Pritchard, B. R. Brooks, H. F. I. Schaefer, A. Y. Sokolov, K. Patkowski, A. E. I. DePrince, U. Bozkaya, R. A. King, F. A. Evangelista, J. M. Turney, T. D. Crawford, and C. D. Sherrill, Psi4 1.4: Open-source software for high-throughput quantum chemistry, *The Journal of Chemical Physics* **152**, 184108 (2020).
- [88] C. Rigetti, J. M. Gambetta, S. Poletto, B. L. Plourde, J. M. Chow, A. D. Córcoles, J. A. Smolin, S. T. Merkel, J. R. Rozen, G. A. Keefe, *et al.*, Superconducting qubit in a waveguide cavity with a coherence time approaching 0.1 ms, *Physical Review B—Condensed Matter and Materials Physics* **86**, 100506 (2012).
- [89] H. Smith, R. Gnanadesikan, and J. Hughes, Multivariate analysis of variance (manova), *Biometrics* **18**, 22 (1962).
- [90] R. G. O’Brien and M. K. Kaiser, Manova method for analyzing repeated measures designs: an extensive primer., *Psychological bulletin* **97**, 316 (1985).
- [91] M. J. Anderson, Permutational multivariate analysis of variance (permanova), *Wiley statsref: statistics reference online*, 1 (2014).
- [92] M. J. Anderson, Distance-based tests for homogeneity of multivariate dispersions, *Biometrics* **62**, 245 (2006).
- [93] L. St. S. Wold, *et al.*, Analysis of variance (anova), *Chemometrics and intelligent laboratory systems* **6**, 259 (1989).
- [94] R. De Maesschalck, D. Jouan-Rimbaud, and D. L. Massart, The mahalanobis distance, *Chemometrics and intelligent laboratory systems* **50**, 1 (2000).
- [95] D. G. Pereira, A. Afonso, and F. M. Medeiros, Overview of friedman’s test and post-hoc analysis, *Communications in Statistics-Simulation and Computation* **44**, 2636 (2015).
- [96] M. G. Kendall and B. B. Smith, The problem of m rankings, *The annals of mathematical statistics* **10**, 275 (1939).
- [97] M. Friedman, A comparison of alternative tests of significance for the problem of m rankings, *The annals of mathematical statistics* **11**, 86 (1940).
- [98] R. F. Woolson, Wilcoxon signed-rank test, *Wiley encyclopedia of clinical trials*, 1 (2007).
- [99] S. Holm, A simple sequentially rejective multiple test procedure, *Scandinavian journal of statistics*, 65 (1979).
- [100] R. Bender and S. Lange, Adjusting for multiple testing—when and how?, *Journal of clinical epidemiology* **54**, 343 (2001).
- [101] S. Illésová, M. Beseda, B. Senjean, V. Novak, and T. Bezdek, Statistical benchmarking of optimization methods for variational quantum eigensolver under quantum noise — replication package, Zenodo (2025), includes the exact Git commit version and environment for replication.
- [102] N. Hansen, S. D. Müller, and P. Koumoutsakos, Reducing the time complexity of the derandomized evolution strategy with covariance matrix adaptation (cma-es), *Evolutionary computation* **11**, 1 (2003).
- [103] M. J. Powell *et al.*, The bobyqa algorithm for bound constrained optimization without derivatives, *Cambridge NA Report NA2009/06*, University of Cambridge, Cambridge **26**, 26 (2009).
- [104] R. Garnett, *Bayesian optimization* (Cambridge University Press, 2023).
- [105] D. P. Kingma, Adam: A method for stochastic optimization, *arXiv preprint arXiv:1412.6980* (2014).
- [106] K. V. Mardia, Measures of multivariate skewness and kurtosis with applications, *Biometrika* **57**, 519 (1970).
- [107] G. E. Box, Non-normality and tests on variances, *Biometrika* **40**, 318 (1953).
- [108] H. Levene, Robust tests for equality of variances, *Contributions to probability and statistics*, 278 (1960).
- [109] M. B. Brown and A. B. Forsythe, Robust tests for the equality of variances, *Journal of the American statistical association* **69**, 364 (1974).
- [110] Y. Benjamini and Y. Hochberg, Controlling the false discovery rate: a practical and powerful approach to multiple testing, *Journal of the Royal statistical society: series B (Methodological)* **57**, 289 (1995).

Appendix A: Optimizer Settings

The overview of the optimization methods is described in Table XI, while their settings are further described here, to facilitate the reproducibility of the results. The maximum number of iterations for each state-averaged VQE phase is set to 500 for all optimizers except iSOMA. The `ftol` parameter is set to 10^{-8} for intended accuracy, for BFGS and SLSQP. iSOMA needed a different set of

parameters, and all can be seen in the Table XII.

TABLE XI. Overview of the optimization methods

Method	Type	Grad.	Constr.	Scope
BFGS	Quasi-Newton	Yes	No	Local
SLSQP	Quadratic programming	Yes	Eq./Ineq.	Local
NM	Direct search	No	No	Local
PM	Line search	No	No	Local
COBYLA	Trust-region	No	Eq./Ineq.	Local
iSOMA	Population-based	No	Heuristic	Global

TABLE XII. Optimizer settings used in this study.

Optimizer	Settings
BFGS	maxiter = 500, ftol = 10^{-8}
COBYLA	maxiter = 500
SLSQP	maxiter = 500, ftol = 10^{-8}
NM	maxiter = 500
PM	maxiter = 500
iSOMA	N_jump = 10, Step = 0.11, PopSize = 25, Max_Migration = 30, Max_FEs = 750, VarMin = -2π , VarMax = 2π , $m = 15$, $n = 5$, $k = 10$

Appendix B: MANOVA

The null hypothesis for MANOVA in two dimensions, which are represented by the ground and excited energies, is defined as

$$H_0 : \boldsymbol{\mu}_1 = \boldsymbol{\mu}_2 = \dots = \boldsymbol{\mu}_g \quad (\text{B1})$$

where $\boldsymbol{\mu}_i \in \mathbb{R}^2$ is the mean vector of group i and g is the number of groups. The groups are the individual noise type setting, each consisting of ten runs.

The MANOVA has three main assumptions that have to be met to allow for this type of statistical analysis. These are the assumptions of normality, homogeneity, and independence.

For the first assumption, of normality, we have chosen Mardia's test [106] to check for multivariate normality, as our data consists of a tuple of ground and excited state energy. The Mardia's test and its results are described in detail in section E.

Now, let us examine the second assumption for the MANOVA approach, i.e., the assumption of homogeneity. This assumption was tested by the following three tests.

Box's M test [107] compares the equality of covariance matrices of all settings. It is defined as

$$M = (N - g) \ln|\mathbf{S}_p| - \sum_{i=1}^g (n_i - 1) \ln|\mathbf{S}_i|, \quad (\text{B2})$$

where $N = \sum_{i=1}^g n_i$ is the total sample size, n_i is the number of samples in the group g_i , g is the number of

groups, $|\cdot|$ denotes the determinant, \mathbf{S}_i is the sample covariance matrix of group i , and \mathbf{S}_p is the pooled covariance matrix,

$$\mathbf{S}_p = \frac{1}{N - g} \sum_{i=1}^g (n_i - 1) \mathbf{S}_i. \quad (\text{B3})$$

The statistic M is approximately χ^2 distributed under the null hypothesis that all group covariance matrices are equal, $H_0 : \boldsymbol{\Sigma}_1 = \boldsymbol{\Sigma}_2 = \dots = \boldsymbol{\Sigma}_g$.

And the null hypothesis for Box's M test for equality of covariance matrices is defined as

$$H_0 : \boldsymbol{\Sigma}_1 = \boldsymbol{\Sigma}_2 = \dots = \boldsymbol{\Sigma}_g \quad (\text{B4})$$

where $\boldsymbol{\Sigma}_i \in \mathbb{R}^{2 \times 2}$ is the covariance matrix of group i .

Here, the results are in Table XIII, and we can observe that the Box's M test was significant for all optimization methods, with $p < 0.001$ in each case, indicating that the assumption of equality of covariance matrices was violated throughout. That said, the equality of group variances was tested next.

TABLE XIII. Box's M test of equality of covariance matrices across optimization methods. p -values are shown directly; significance threshold is $p > 0.001$.

Method	M	χ^2	df	p
BFGS	1058	969.3	60	< 0.001
COBYLA	589.2	539.7	60	< 0.001
PM	1068	977.3	60	< 0.001
SLSQP	1278	1167	60	< 0.001
NM	724.7	663.8	60	< 0.001
iSOMA	698.7	639.9	60	< 0.001

Levene's test [108] evaluates the equality of group variances. For each observation Y_{ij} in group i , the transformed score is

$$Z_{ij} = |Y_{ij} - \bar{Y}_i|, \quad (\text{B5})$$

where \bar{Y}_i is the group mean. The null hypothesis for equality of variances is defined as

$$H_0 : \sigma_1^2 = \sigma_2^2 = \dots = \sigma_g^2 \quad (\text{B6})$$

where σ_i^2 is the variance of a single coordinate in group i .

The results for Levene's test are visible in Table XIV. The columns report the optimization method, the Levene's test statistic (F) for the x - and y -axis variables (F_x, F_y), and their corresponding p -values (p_x, p_y). And it was also significant for both the x and y axes across all optimization methods, with $p < 0.05$ in every case, showing that the assumption of homogeneity of variances was not satisfied.

The last test done for the second assumption of MANOVA was the Brown-Forsythe test [109]. It is a median-based modification of Levene's test, which improves robustness under non-normality and was chosen

TABLE XIV. Levene’s test of equality of variances across optimization methods. p -values are shown directly; significance threshold is $p > 0.05$.

Method	F_x	p_x	F_y	p_y
BFGS	8.026	1.57×10^{-16}	4.976	9.592×10^{-10}
COBYLA	5.186	3.081×10^{-10}	7.425	2.947×10^{-15}
PM	7.697	8.165×10^{-16}	9.257	5.227×10^{-19}
SLSQP	13.47	1.692×10^{-26}	13.57	1.14×10^{-26}
NM	13.63	5.48×10^{-27}	5.534	4.802×10^{-11}
iSOMA	20.25	8.8×10^{-37}	4.596	7.572×10^{-9}

because of the non-normality in the case of the *ideal* family. The transformed scores are defined as

$$Z_{ij} = |Y_{ij} - \tilde{Y}_i|, \quad (\text{B7})$$

where \tilde{Y}_i is the group median. The null hypothesis for the Brown-Forsythe test is defined as

$$H_0 : \sigma_1^2 = \sigma_2^2 = \dots = \sigma_g^2 \quad (\text{B8})$$

where σ_i^2 is the variance about the group median for group i .

We apply both tests because Levene’s test provides a general assessment of variance equality, while the Brown-Forsythe variant offers a more robust check against non-normality, allowing us to confirm that any detected heterogeneity is not driven by outliers or deviations from normality.

The results are shown in Table XV. And we see that the test was significant for both the x and y axes across all optimization methods, with $p < 0.05$ in every case, indicating heterogeneity of variances even under the more robust median-based approach.

TABLE XV. Brown–Forsythe test of equality of variances across optimization methods. p -values are shown directly; significance threshold is $p > 0.05$.

Method	F_x	p_x	F_y	p_y
BFGS	6.294	8.947×10^{-13}	4.135	9.467×10^{-8}
COBYLA	2.731	2.073×10^{-4}	6.604	1.817×10^{-13}
PM	5.751	1.572×10^{-11}	5.689	2.185×10^{-11}
SLSQP	10.46	3.212×10^{-21}	8.993	2.167×10^{-18}
NM	7.493	2.099×10^{-15}	4.680	4.775×10^{-9}
iSOMA	5.897	7.088×10^{-12}	2.609	3.977×10^{-4}

From the three tests described above, we can summarize that the assumption of homogeneity was not met, as there is significant heterogeneity across groups. While we can already observe that the MANOVA will not be suitable for our case, for the sake of completeness, let us state that the third assumption of independence holds, as all runs were calculated independently of each other, with different random seeds.

Appendix C: PERMDISP

The null hypothesis for the one-way ANOVA used inside PERMDISP is defined as

$$H_0 : \mu_1 = \mu_2 = \dots = \mu_g \quad (\text{C1})$$

where μ_i is the mean of the distance-to-centroid values for group i .

Significance is assessed by permutations of the residuals under a reduced model. The null hypothesis is defined as

$$H_0 : \delta_1 = \delta_2 = \dots = \delta_g \quad (\text{C2})$$

where $\delta_i = \mathbb{E}[d(\mathbf{x}, \bar{\mathbf{x}}_i)]$ is the mean distance of observations to the centroid $\bar{\mathbf{x}}_i$ of group i .

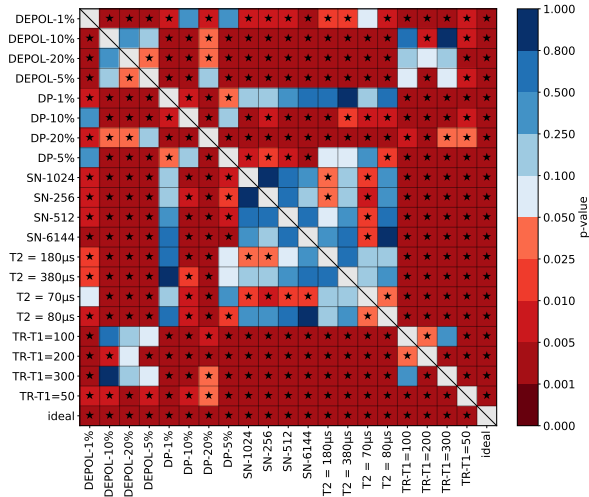
This means that groups have equal multivariate dispersions, and if it holds, then the differences detected by PERMANOVA can be attributed solely to differences in group centroids rather than unequal spread of the data. If the null hypothesis is rejected, then the PERMANOVA can be conducted, but with the interpretation of the results, the fact that the spread of the data can cause the differences has to be taken into account.

The results of PERMDISP analysis are shown in Table XVI and in Figure 7. The columns report the optimization method, the PERMDISP F -statistic, the associated degrees of freedom (df), and the permutation-based p -value. The test was significant for all optimization methods, with $p < 0.05$ in every case, indicating heterogeneity of multivariate dispersions across groups. This tells us that significant PERMANOVA results may arise from differences in group dispersions rather than differences in centroid locations.

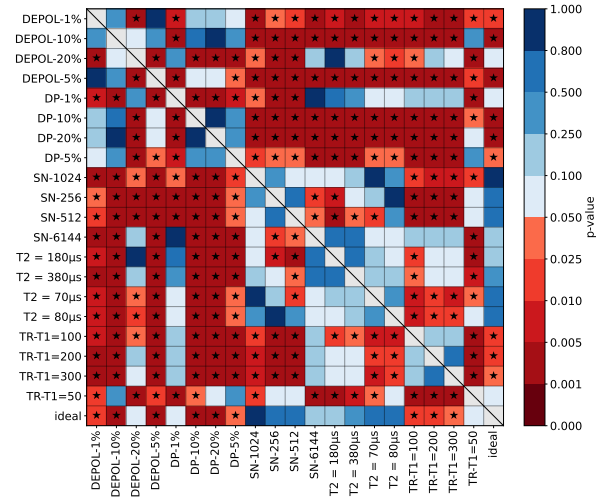
TABLE XVI. PERMDISP test of homogeneity of multivariate dispersions across optimization methods. All tests are based on Euclidean distances with 10,000 permutations. Significance threshold is $p > 0.05$.

Method	F	df	p
BFGS	16.66	(20, 189)	< 0.0001
COBYLA	11.27	(20, 189)	< 0.0001
PM	12.94	(20, 188)	< 0.0001
SLSQP	30.20	(20, 185)	< 0.0001
NM	8.11	(20, 189)	0.0003
iSOMA	16.66	(20, 189)	< 0.0001

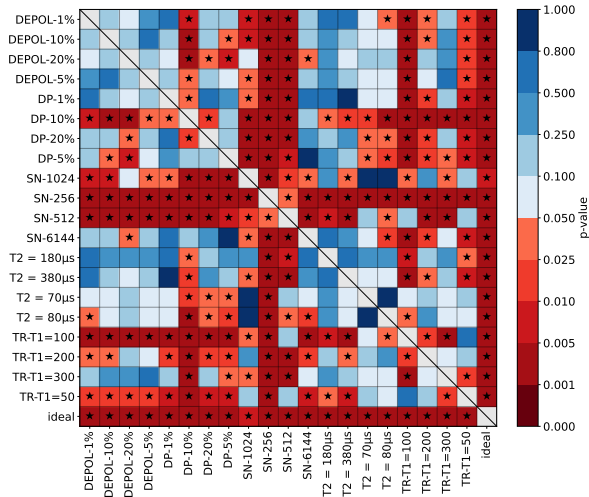
The figures visualize the distances of individual SA-OO-VQE results from their corresponding group centroids in the $(E_{\text{gs}}, E_{\text{es}})$ space, thereby illustrating the relative multivariate dispersion under different noise models and optimization methods. These visualizations are intended to complement the permutation-based PERMDISP statistics reported in the main body and should be interpreted together with those quantitative results.



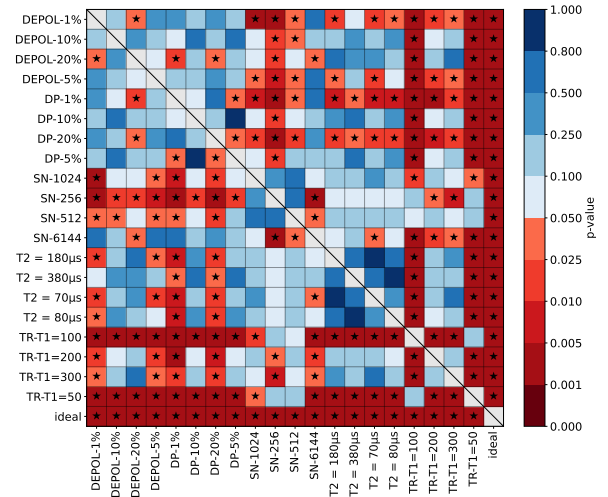
(a) SLSQP



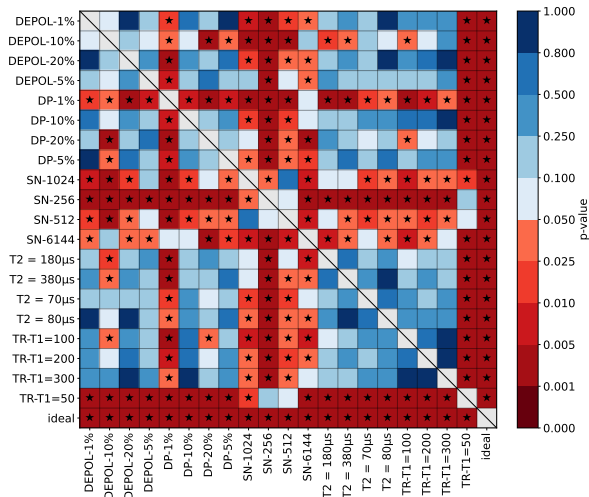
(b) iSOMA



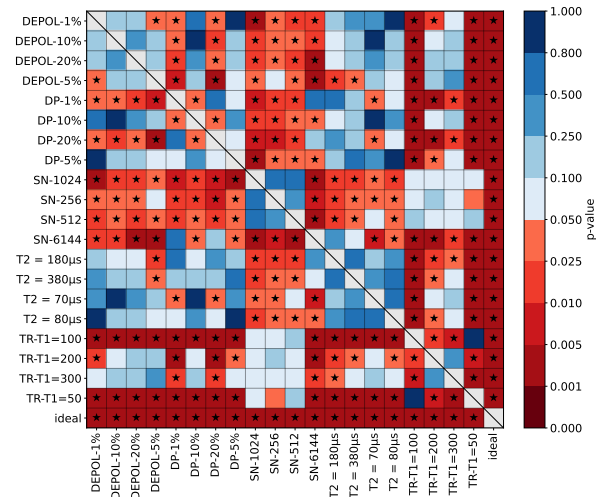
(c) PM



(d) NM



(e) COBYLA



(f) BFGS

FIG. 7. Pairwise PERMDISP tests for homogeneity of multivariate dispersions across different noise settings for all optimization methods. Cells show p -values. Significant values indicate unequal within-family dispersion, which may confound PERMANOVA results. The diagonal is masked.

Appendix D: PERMANOVA

For the PERMANOVA, the Euclidean distance defined by

$$d(x_i, x_j) = \sqrt{\sum_{k=1}^p (x_{ik} - x_{jk})^2} \quad (\text{D1})$$

was chosen, where x_i and x_j are observations in p -dimensional space.

The null hypothesis for PERMANOVA testing equality of centroids is defined as

$$H_0 : \boldsymbol{\mu}_1 = \boldsymbol{\mu}_2 = \dots = \boldsymbol{\mu}_g \quad (\text{D2})$$

where $\boldsymbol{\mu}_i$ is the multivariate centroid of group i under the Euclidean distance.

The results of the PERMANOVA are presented in Table XVII. The columns report the optimization method, the PERMANOVA pseudo- F statistic, the associated degrees of freedom, the permutation-based p -value, and the proportion of explained variance (R^2). The pseudo- F statistic is defined as the ratio between the mean squares among groups and the mean squares within groups,

$$F = \frac{SS_{\text{between}}/(k-1)}{SS_{\text{within}}/(N-k)}, \quad (\text{D3})$$

where SS_{between} and SS_{within} are the sums of squared distances among group centroids and within groups, respectively, k is the number of groups, and N is the total number of observations. These sums of squares are computed directly from the distance matrix rather than from the raw data, which allows the test to be applied to any distance or dissimilarity measure. Larger values of the pseudo- F statistic indicate that the distances between group centroids are greater relative to the dispersion within groups. Statistical significance is determined by randomly permuting group labels to generate the null distribution of F , from which the permutation-based p -value is obtained.

Significant effects were detected by PERMANOVA, shown in Figure 8, for all optimization methods as p -values were all below 0.001, indicating that the distributions of results obtained with different estimators differ significantly in multivariate space. However, because the PERMDISP test yielded significant results as well as all p -values were below 0.003, it is not yet possible to determine whether the observed differences are due to distinct group centroids, location effects, unequal dispersions, or variance heterogeneity.

To address these issues, a post hoc tests were performed, in this case in the form of pairwise PERMANOVA and PERMDISP, so that the results can be compared and summarized. The results were then adapted by Benjamini-Hochberg correction [110], which was chosen to better capture the real differences and their statistical significance.

TABLE XVII. PERMANOVA results across optimization methods. p -values are obtained by permutation with 10,000 permutations; significance threshold is $p > 0.05$.

Method	Pseudo- F	df	p	R^2
BFGS	252.4 (20, 189)	< 0.0001	0.9639	
COBYLA	6466 (20, 189)	< 0.0001	0.9985	
PM	3871 (20, 188)	< 0.0001	0.9976	
SLSQP	23.25 (20, 185)	< 0.0001	0.7154	
NM	7774 (20, 189)	< 0.0001	0.9988	
iSOMA	252.4 (20, 189)	< 0.0001	0.9639	

The null hypothesis for pairwise PERMANOVA comparing different settings is defined as

$$H_0 : \boldsymbol{\mu}_a = \boldsymbol{\mu}_b \quad (\text{D4})$$

where $\boldsymbol{\mu}_a$ and $\boldsymbol{\mu}_b$ are the multivariate centroids of families a and b .

Furthermore, the null hypothesis for pairwise PERMDISP comparing two different settings is defined as

$$H_0 : \delta_a = \delta_b \quad (\text{D5})$$

where δ_a and δ_b are the mean distances to centroids for families a and b .

The results for the Post Hoc test for BFGS are visualized in Figure 7(f), where the pairwise PERMDISP is visualized, Figure 8(f), where the pairwise PERMANOVA results are shown in a heatmap with Benjamini-Hochberg corrections applied. From these figures, we can conclude that for the majority of the pairs, there is a significant location displacement, with the exception of the sampling noise settings pairs and the combination of sampling noise settings with ideal setting and dephasing channel with a level of 1%. From the second figure, we can see that a lot of pairs have unequal dispersion, so in these cases, the dispersion of the clusters plays a significant role.

The same results, but for COBYLA, are visualized in Figure 7(e) for PERMDISP and in Figure 8(e) for the case of PERMANOVA with Benjamini-Hochberg corrections. The exceptions are similar to the BFGS case, particularly among the sampling noise settings and their combinations with the ideal state. Moreover, many pairs also exhibit unequal dispersion, suggesting that group spread differences play an important role in the interpretation of the observed effects under the COBYLA optimization.

For iSOMA the results for pairwise PERMDISP are in Figure 7(b), and for pairwise PERMANOVA in Figure 8(b). These figures demonstrate that most pairs display significant location differences, but there are slightly more pairs that are similar than in the previous two cases.

The results for the post hoc test for NM are visualized in Figure 7(d), where the pairwise PERMDISP outcomes are shown, and in Figure 8(d), where the pairwise PERMANOVA results with Benjamini-Hochberg corrections are presented. Similar to the other optimizers, the

majority of pairs display significant location differences, except for several comparisons within the sampling noise settings, but a new cluster with similarities emerges in the T_2 region.

The results for the post hoc test for PM are visualized in Figure 7(c), where the pairwise PERMDISP results are shown, and in Figure 8(c), where the pairwise PERMANOVA outcomes with Benjamini-Hochberg corrections are presented. The cluster of similarities is extended to the combination of sampling noise with a few categories of T_2 , which is the mean time to dephasing.

The results for the post hoc test for SLSQP are visualized in Figure 7(a), where the pairwise PERMDISP outcomes are shown, and in Figure 8(a), where the pairwise PERMANOVA results with Benjamini-Hochberg corrections are presented. Here, because of the overall bad convergence, most pairs are statistically similar.

Appendix E: Mardia's multivariate normality

The Mardia's test looks at the multivariate skewness of the data

$$b_{1,p} = \frac{1}{n^2} \sum_{i=1}^n \sum_{j=1}^n [(\mathbf{x}_i - \bar{\mathbf{x}})^\top \mathbf{S}^{-1} (\mathbf{x}_j - \bar{\mathbf{x}})]^3, \quad (\text{E1})$$

and their kurtosis

$$b_{2,p} = \frac{1}{n} \sum_{i=1}^n [(\mathbf{x}_i - \bar{\mathbf{x}})^\top \mathbf{S}^{-1} (\mathbf{x}_i - \bar{\mathbf{x}})]^2. \quad (\text{E2})$$

Here, \mathbf{x}_i denotes the i -th observation vector, $\bar{\mathbf{x}}$ the sample mean, and \mathbf{S} the sample covariance matrix. Here, n is the number of observations (data points) within a given group, and each observation vector $\mathbf{x}_i = (E_{0,i}, E_{1,i})^\top$ contains the ground- and excited-state energies obtained in a single run. The sample mean vector $\bar{\mathbf{x}}$ represents the mean of these energies across all observations, and the sample covariance matrix \mathbf{S} is defined as

$$\mathbf{S} = \frac{1}{n-1} \sum_{i=1}^n (\mathbf{x}_i - \bar{\mathbf{x}})(\mathbf{x}_i - \bar{\mathbf{x}})^\top, \quad (\text{E3})$$

which captures both the variances of E_0 and E_1 and their covariance.

The skewness statistic $b_{1,p}$ is approximately distributed as

$$n \cdot b_{1,p} \sim \chi_{\frac{p(p+1)(p+2)}{6}}^2, \quad (\text{E4})$$

here, χ^2 denotes the chi-squared distribution, which serves as the reference distribution for the test under the null hypothesis of multivariate normality.

And the null hypothesis for Mardia's multivariate normality based on skewness is defined as

$$H_0 : b_{1,p} = 0 \quad (\text{E5})$$

where $b_{1,p}$ is Mardia's multivariate skewness and $p = 2$ is the dimensionality.

While the kurtosis statistic is standardized as

$$z_{\text{kurt}} = \frac{b_{2,p} - p(p+2)}{\sqrt{\frac{8p(p+2)}{n}}} \sim \mathcal{N}(0, 1). \quad (\text{E6})$$

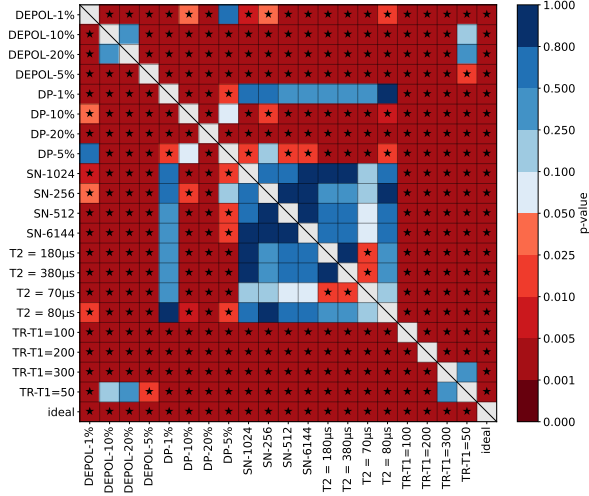
The null hypothesis for Mardia's multivariate normality based on kurtosis is defined as

$$H_0 : b_{2,p} = p(p+2) \quad (\text{E7})$$

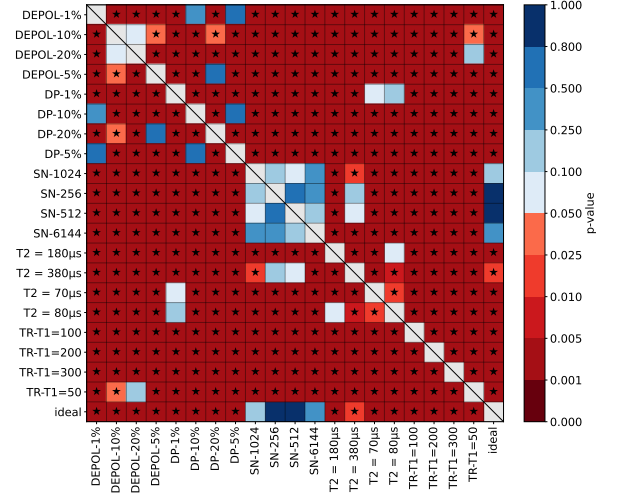
where $b_{2,p}$ is Mardia's multivariate kurtosis and $p = 2$ is the dimensionality.

Non-significant values for both the skewness and kurtosis components ($p > 0.05$) indicate that the data do not significantly deviate from multivariate normality.

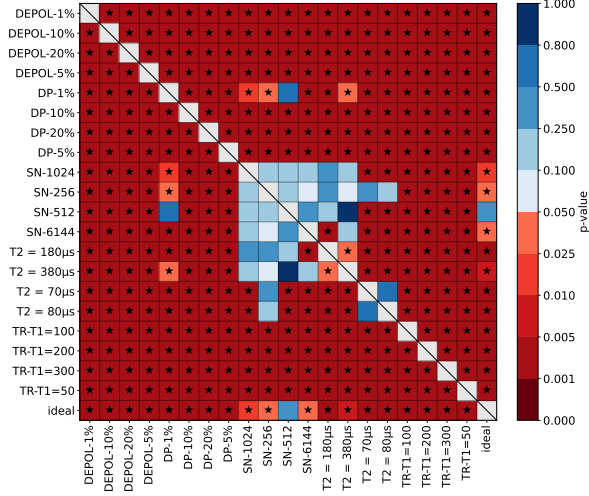
The results of this tests are shown in Tables XVIII to XXIII where the columns indicate the experimental family, Mardia's skewness statistic ($b_{1,p}$), its chi-square test value (χ^2) with corresponding degrees of freedom (df) and p -value (p_{skew}), followed by Mardia's kurtosis statistic ($b_{2,p}$), its standardized z -score (z_{kurt}), and the associated p -value (p_{kurt}). A higher χ^2 value relative to its degrees of freedom indicates a stronger deviation from multivariate symmetry, meaning the data are less consistent with multivariate normality. These results tell us that almost all of the families do not violate the multivariate normality with the following exceptions: for the SLSQP, the *ideal* family fails both in skewness and kurtosis with $p_{\text{skew}} = 0.002$ and $p_{\text{kurt}} = 0.041$. The second violation is in the NM again for the *ideal* family, where the skewness is violated with $p_{\text{skew}} = 0.042$. While these two are the only clear violations of multivariate normality, several other examples came close, especially the *ideal* family in other optimization methods. This shows that the *ideal* family is sensitive and prone to deviations of normality.



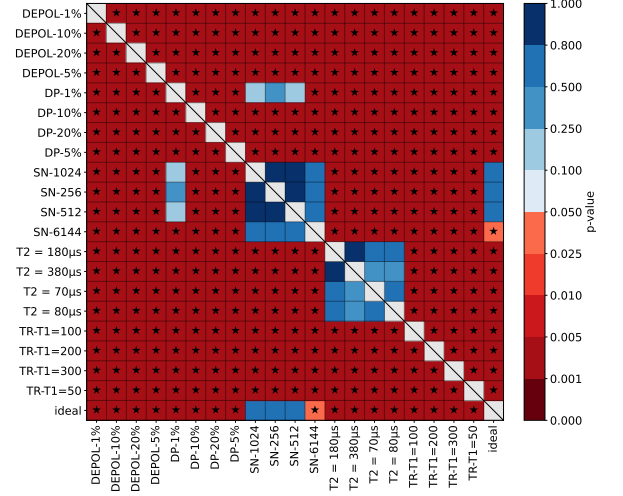
(a) SLSQP



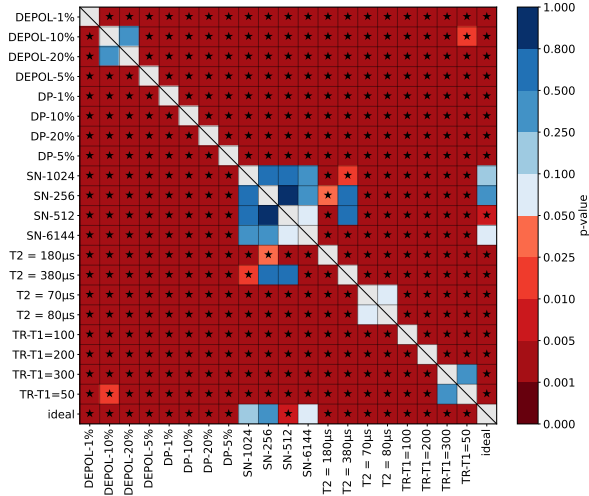
(b) iSOMA



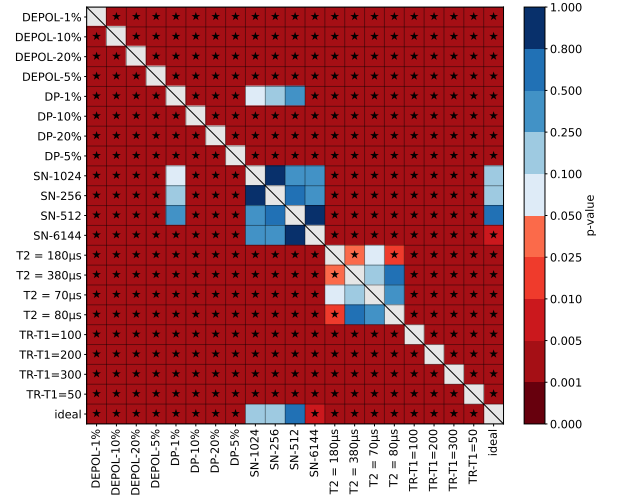
(c) PM



(d) NM



(e) COBYLA



(f) BFGS

FIG. 8. Pairwise PERMANOVA (Euclidean distance) between noise settings for all optimization methods. Cells show Benjamini–Hochberg FDR-adjusted p -values. Warmer colors denote lower p -values, indicating stronger evidence of differences in multivariate location. The diagonal is masked.

TABLE XVIII. Mardia’s multivariate normality test results across all families for BFGS.

family	$b_{1,p}$	χ^2	df	p_{skew}	$b_{2,p}$	z_{kurt}	p_{kurt}
DEPOL-1%	0.704	1.173	4	0.882	4.527	-1.373	0.170
DEPOL-10%	0.633	1.055	4	0.901	4.840	-1.249	0.212
DEPOL-20%	2.420	4.034	4	0.401	6.852	-0.454	0.650
DEPOL-5%	0.418	0.697	4	0.952	4.398	-1.424	0.155
DP-1%	1.373	2.288	4	0.683	5.521	-0.980	0.327
DP-10%	0.200	0.333	4	0.988	4.836	-1.251	0.211
DP-20%	1.327	2.211	4	0.697	5.524	-0.979	0.328
DP-5%	0.260	0.433	4	0.980	4.605	-1.342	0.180
SN-1024	0.947	1.579	4	0.813	5.298	-1.068	0.286
SN-256	1.603	2.672	4	0.614	5.350	-1.047	0.295
SN-512	0.251	0.419	4	0.981	4.495	-1.385	0.166
SN-6144	1.274	2.123	4	0.713	4.577	-1.353	0.176
T2=180 μ s	1.579	2.631	4	0.621	6.069	-0.763	0.445
T2=380 μ s	1.025	1.708	4	0.789	6.541	-0.577	0.564
T2=70 μ s	0.838	1.397	4	0.845	5.218	-1.100	0.272
T2=80 μ s	0.519	0.865	4	0.930	5.744	-0.892	0.373
TR-T1=100	0.763	1.271	4	0.866	6.084	-0.758	0.449
TR-T1=200	0.555	0.926	4	0.921	4.488	-1.388	0.165
TR-T1=300	0.209	0.348	4	0.987	5.012	-1.181	0.238
TR-T1=50	1.770	2.951	4	0.566	4.928	-1.214	0.225
ideal	5.184	8.640	4	0.071	6.570	-0.565	0.572

TABLE XIX. Mardia’s multivariate normality test results across all families for PM.

family	$b_{1,p}$	χ^2	df	p_{skew}	$b_{2,p}$	z_{kurt}	p_{kurt}
DEPOL-1%	0.4354	0.726	4	0.948	4.823	-1.256	0.209
DEPOL-10%	0.5162	0.860	4	0.930	4.406	-1.421	0.155
DEPOL-20%	1.574	2.624	4	0.623	5.262	-1.082	0.279
DEPOL-5%	2.943	4.904	4	0.297	6.772	-0.486	0.627
DP-1%	0.6806	1.134	4	0.889	5.143	-1.129	0.259
DP-10%	1.506	2.510	4	0.643	4.837	-1.250	0.211
DP-20%	1.838	3.063	4	0.547	6.659	-0.530	0.596
DP-5%	1.485	2.476	4	0.649	5.454	-1.006	0.314
SN-1024	5.070	8.449	4	0.076	8.171	0.067	0.946
SN-256	0.912	1.520	4	0.823	4.795	-1.267	0.205
SN-512	2.754	4.589	4	0.332	6.556	-0.620	0.535
SN-6144	2.384	3.973	4	0.410	6.265	-0.686	0.493
T2=180 μ s	2.474	3.711	4	0.447	6.178	-0.683	0.494
T2=380 μ s	0.526	0.877	4	0.928	4.766	-1.278	0.201
T2=70 μ s	3.003	5.005	4	0.287	7.047	-0.377	0.706
T2=80 μ s	1.378	2.297	4	0.681	6.036	-0.776	0.438
TR-T1=100	0.620	1.033	4	0.905	5.534	-0.975	0.330
TR-T1=200	0.630	1.050	4	0.902	5.335	-1.054	0.292
TR-T1=300	1.162	1.937	4	0.747	5.327	-1.057	0.291
TR-T1=50	1.277	2.129	4	0.712	6.659	-0.530	0.596
ideal	5.184	8.640	4	0.071	6.570	-0.565	0.572

family	$b_{1,p}$	χ^2	df	p_{skew}	$b_{2,p}$	z_{kurt}	p_{kurt}
DEPOL-1%	0.898	1.497	4	0.827	4.070	-1.553	0.120
DEPOL-10%	0.579	0.965	4	0.915	4.444	-1.406	0.160
DEPOL-20%	0.586	0.977	4	0.913	5.307	-1.064	0.287
DEPOL-5%	0.772	1.287	4	0.864	5.284	-1.074	0.283
DP-1%	1.461	2.434	4	0.656	4.833	-1.252	0.211
DP-10%	0.398	0.664	4	0.956	5.045	-1.168	0.243
DP-20%	1.992	3.320	4	0.506	6.500	-0.593	0.553
DP-5%	1.931	3.218	4	0.522	6.844	-0.457	0.648
SN-1024	0.303	0.505	4	0.973	4.070	-1.554	0.120
SN-256	1.515	2.526	4	0.640	4.368	-1.436	0.151
SN-512	0.529	0.881	4	0.927	5.300	-1.065	0.287
SN-6144	1.060	1.767	4	0.778	4.004	-1.579	0.114
T2 = 180 μ s	0.162	0.270	4	0.992	4.394	-1.425	0.154
T2 = 380 μ s	0.116	0.135	4	0.998	3.765	-1.401	0.161
T2 = 70 μ s	0.539	0.899	4	0.925	4.110	-1.538	0.124
T2 = 80 μ s	0.086	0.144	4	0.998	3.852	-1.639	0.101
TR-T1=100	0.230	0.383	4	0.984	5.112	-1.142	0.254
TR-T1=200	0.228	0.343	4	0.987	4.615	-1.269	0.204
TR-T1=300	0.128	0.214	4	0.995	3.918	-1.613	0.107
TR-T1=50	0.734	1.223	4	0.874	4.855	-1.243	0.214
ideal	10.390	17.310	4	0.002	13.160	2.041	0.041

TABLE XX. Mardia’s multivariate normality test results across all families for SLSQP.

family	$b_{1,p}$	χ^2	df	p_{skew}	$b_{2,p}$	z_{kurt}	p_{kurt}
DEPOL-1%	0.704	1.173	4	0.883	4.527	-1.373	0.170
DEPOL-10%	0.633	1.055	4	0.901	4.840	-1.249	0.212
DEPOL-20%	2.420	4.034	4	0.402	6.852	-0.454	0.650
DEPOL-5%	0.418	0.697	4	0.952	4.398	-1.424	0.155
DP-1%	1.373	2.288	4	0.683	5.521	-0.980	0.327
DP-10%	0.200	0.333	4	0.988	4.836	-1.251	0.211
DP-20%	1.327	2.211	4	0.697	5.524	-0.979	0.328
DP-5%	0.260	0.433	4	0.980	4.605	-1.342	0.180
SN-1024	0.947	1.579	4	0.813	5.298	-1.068	0.286
SN-256	1.603	2.672	4	0.614	5.350	-1.047	0.295
SN-512	0.251	0.419	4	0.981	4.495	-1.385	0.166
SN-6144	1.274	2.123	4	0.713	4.577	-1.353	0.176
T2=180 μ s	1.579	2.631	4	0.621	6.069	-0.763	0.445
T2=380 μ s	1.025	1.708	4	0.789	6.541	-0.577	0.564
T2=70 μ s	0.838	1.397	4	0.845	5.218	-1.100	0.272
T2=80 μ s	0.519	0.865	4	0.930	5.744	-0.892	0.373
TR-T1=100	0.763	1.271	4	0.866	6.084	-0.758	0.449
TR-T1=200	0.555	0.926	4	0.921	4.488	-1.388	0.165
TR-T1=300	0.209	0.348	4	0.987	5.012	-1.181	0.238
TR-T1=50	1.770	2.951	4	0.566	4.928	-1.214	0.225
ideal	5.184	8.640	4	0.071	6.570	-0.565	0.572

TABLE XXI. Mardia’s multivariate normality test results across all families for COBYLA.

TABLE XXII. Mardia’s multivariate normality test results across all families for NM.

family	$b_{1,p}$	χ^2	df	p_{skew}	$b_{2,p}$	z_{kurt}	p_{kurt}
DEPOL-1%	0.8959	1.493	4	0.8279	5.433	-1.015	0.3103
DEPOL-10%	3.5900	5.984	4	0.2004	8.629	0.249	0.8037
DEPOL-20%	1.8290	3.048	4	0.5499	5.948	-0.811	0.4174
DEPOL-5%	1.4560	2.427	4	0.6577	6.254	-0.690	0.4901
DP-1%	0.6382	1.064	4	0.9000	4.221	-1.494	0.1352
DP-10%	0.9936	1.656	4	0.7987	5.946	-0.812	0.4167
DP-20%	3.3270	5.545	4	0.2358	7.403	-0.236	0.8133
DP-5%	0.2449	0.408	4	0.9818	3.979	-1.589	0.1120
SN-1024	3.4810	5.802	4	0.2144	7.349	-0.258	0.7968
SN-256	0.5821	0.970	4	0.9143	5.503	-0.987	0.3236
SN-512	3.0700	5.117	4	0.2755	7.192	-0.319	0.7495
SN-6144	1.4270	2.378	4	0.6665	6.460	-0.609	0.5426
T2 = 180 μ s	0.3522	0.587	4	0.9645	4.547	-1.365	0.1723
T2 = 380 μ s	1.0610	1.768	4	0.7783	5.285	-1.073	0.2831
T2 = 70 μ s	1.3240	2.207	4	0.6977	5.215	-1.101	0.2709
T2 = 80 μ s	0.2159	0.360	4	0.9856	4.534	-1.370	0.1707
TR-T1=100	0.5788	0.965	4	0.9151	4.670	-1.316	0.1881
TR-T1=200	1.2070	2.012	4	0.7335	5.960	-0.807	0.4199
TR-T1=300	1.5010	2.501	4	0.6445	5.431	-1.016	0.3098
TR-T1=50	0.4782	0.797	4	0.9388	3.989	-1.585	0.1129
ideal	5.9360	9.894	4	0.0423	10.030	0.801	0.4232

TABLE XXIII. Mardia’s multivariate normality test results for iSOMA.

family	$b_{1,p}$	χ^2	df	p_{skew}	$b_{2,p}$	z_{kurt}	p_{kurt}
DEPOL-1%	5.149	8.582	4	0.07245	7.764	-0.09337	0.9256
DEPOL-10%	3.717	6.195	4	0.1851	7.060	-0.3715	0.7103
DEPOL-20%	1.037	1.729	4	0.7855	5.487	-0.9933	0.3206
DEPOL-5%	1.692	2.820	4	0.5884	4.273	-1.473	0.1407
DP-1%	3.509	5.849	4	0.2107	8.402	0.1588	0.8738
DP-10%	3.302	5.504	4	0.2394	6.863	-0.4496	0.6530
DP-20%	0.908	1.514	4	0.8242	5.000	-1.186	0.2357
DP-5%	2.594	4.323	4	0.3640	7.203	-0.3152	0.7526
SN-1024	1.558	2.597	4	0.6274	5.604	-0.9472	0.3435
SN-256	0.266	0.443	4	0.9788	4.590	-1.348	0.1777
SN-512	1.010	1.684	4	0.7937	5.010	-1.182	0.2372
SN-6144	4.216	7.027	4	0.1345	7.763	-0.0939	0.9252
T2=180 μ s	2.781	4.634	4	0.3269	6.833	-0.4615	0.6445
T2=380 μ s	2.674	4.457	4	0.3476	7.679	-0.1270	0.8990
T2=70 μ s	0.173	0.288	4	0.9906	4.836	-1.251	0.2111
T2=80 μ s	1.769	2.948	4	0.5666	6.639	-0.5378	0.5907
TR-T1=100	1.646	2.743	4	0.6018	5.731	-0.8968	0.3698
TR-T1=200	1.941	3.236	4	0.5192	6.705	-0.5118	0.6088
TR-T1=300	1.389	2.314	4	0.6782	6.106	-0.7486	0.4541
TR-T1=50	2.147	3.579	4	0.4660	6.139	-0.7355	0.4620
ideal	4.799	7.998	4	0.09166	8.690	0.2729	0.7849